

NASA SCIENCE MISSION DIRECTORATE

Applied Sciences Program Air Quality Program Element

Final Report: Experiment to Improve Air-Quality Forecasts with NASA Satellite Observations

**Contract #: NNM05AA22A
Account #: 745275 (5-24176)
Proposal No. 2007-311**

Authors:

**Arastoo Biazar, UAHuntsville
Kirk Fuller, UAHuntsville
Maudood Khan, USRA/MSFC
William Koshak, MSFC
Michael Newchurch, UAHuntsville
Yun Hee Park, UAHuntsville
Lihua Wang, UAHuntsville**

Date Submitted: September 11, 2009



*Expanding and accelerating the realization of economic and societal
benefits from Earth-Sun System science, information, and technology*

Table of Contents

A. Executive Summary	3
B. Project Description	3
C. Decision Support System Overview	3
1. Background.....	3
2. DSS components.....	4
3. Systems engineering approach	4
D. NASA Earth Science research products.....	5
E. Description of the modeling experiment.....	5
1. General Overview	5
2. Air quality modeling (CMAQ-CTM) configuration	5
3. Meteorological modeling.....	6
4. Emissions processing	10
5. Pre-processing of satellite/ozonesonde data	11
5a. Processing of ozonesonde and OMI satellite observations for CMAQ-CTM.....	11
5b. Processing of Aerosol Optical Depth (AOT) from MODIS	13
5c. Processing of global model data for CMAQ-CTM.....	18
F. Model performance evaluation	25
G. Conclusions and recommendation for future research and applications	48

A. Executive Summary

This Rapid Prototyping Capability (RPC) project uses NASA research satellite ozone and aerosol products from AURA/OMI and Terra/MODIS as boundary and initial conditions for Community Multi-scale Air-Quality (CMAQ) calculations of air quality over the U.S. in August 2006. The extensive ozonesonde observations during IONS06 and the EPA surface network provide validation data for chemical model evaluation while the national meteorological networks provide evaluation data for the physical model calculations.

Satellite observations constrained CMAQ either directly from the satellite fields or from the RAQMS CTM that had assimilated total ozone fields from OMI. Using the NASA satellite data results in improved model calculation of aerosols in the boundary layer and improved ozone, especially in the middle and upper troposphere but also some small improvement in the boundary layer. Use of additional satellite data (e.g. NO₂ and HCHO) could provide further improvements.

B. Project Description

The overall goal of the Rapid Prototyping Capability (RPC) is to provide for an accelerated simulation and testing of candidate configurations with current and future Earth observation mission measurements and research results in accordance with NASA's 2006 Strategic Plan: "NASA's Applied Sciences program will continue the Agency's efforts in benchmarking the assimilation of NASA research results into policy and management decision-support tools that are vital for the Nation's environment, economy, safety, and security."

The specific purpose of this RPC Experiment is to design an air-quality forecasting system (consisting of Georgia Environmental Protection Division, Air Protection Branch CMAQ model decision tool, NASA Earth Science Research Results (NESRR) from AURA/OMI, AQUA and Terra/MODIS and test its *feasibility and value (F&V)*.

C. Decision Support System Overview

1. Background

Established through an act of Congress (i.e., Clean Air Act or CAA) in 1970, the U.S. Environmental Protection Agency (EPA) is the federal entity responsible for protecting public health through development and enforcement of environmental standards. Over the years, the U.S. EPA has established a sophisticated and reliable air quality monitoring network and an extensive array of statistical, analytical, and physical models. These data, models, and analysis tools collectively represent our understanding of human activities and natural processes, which govern the generation, transport, and transformation of pollutants in the atmosphere. The Air Quality Management Decision Support System (AQMDSS), a computational framework, contains the individual elements that form the basis for the proposal. Generally, AQMDSS comprises of a mesoscale atmospheric model, an air quality model, and an emissions model. Federal, state, and local agencies, and other stakeholders extensively use the system for development and evaluation of emission control strategies (i.e. State Implementation Plans or SIPs) aimed at improving air quality and protecting public health. They also provide short-term forecasts of air pollution events that might pose a health hazard for the public, as well as sensitive groups (e.g., children, elderly). State and local agencies routinely use the modeling results to issue health advisories. The Air Protection Branch (APB) of the Georgia Environmental Protection Division (EPD), a participant in this study, issues daily air quality (i.e., ozone and particulate matter) forecasts using results from CMAQ-CTM. The study will demonstrate operational viability and scientific necessity for assimilating satellite-based measurements of gas and aerosol species within Air Quality Models (AQMs), which are an important component of AQMDSS.

2. DSS components

The subject of this research, AQMDSS, is comprised of Community Multi-scale Air Quality (CMAQ) Chemical Transport Model (CTM) or Models-3; Mesoscale Meteorological model (MM5); and Sparse Matrix Operating Kernel for Emissions (SMOKE). Dynamical data assimilating meteorological models (also referred to as mesoscale models) such as MM5 or WRF (Weather Research Forecast) generally supply meteorological fields for CMAQ-CTM. Meteorology Chemistry Interface Processor (MCIP) creates input files for CMAQ-CTM. Its main function is to read meteorological fields simulated by the mesoscale model, compute dry deposition velocities, and other variables that CMAQ-CTM needs but are not available from the mesoscale model, and output data in Models-3 IOAPI format. The SMOKE emissions processor, which is capable of processing emissions from anthropogenic (i.e., area, non-road, on-road, point) and biogenic sources, creates gridded, temporalized, and speciated emission files required by CMAQ-CTM. A variety of agencies and organizations including Clean Air Markets Division and Technology Transfer Network of EPA, California Air Resources Board, and Texas Commission on Environmental Quality supply the emission inventories and associated input.

3. Systems engineering approach

Although satellite products undergo extensive quality assurance checks, we consider it prudent to design and develop an integrated model-observation system with additional quality checks. Major challenges in using NASA satellite data within CMAQ-CTM include excessive loss of data due to cloud contamination, and low temporal resolution, since polar orbiting satellites record data over a particular point once or twice a day. Hence, we have developed a series of quality control and re-sampling algorithms, as well as software that will allow re-gridding of satellite data onto the modeling grid (Figure 1).

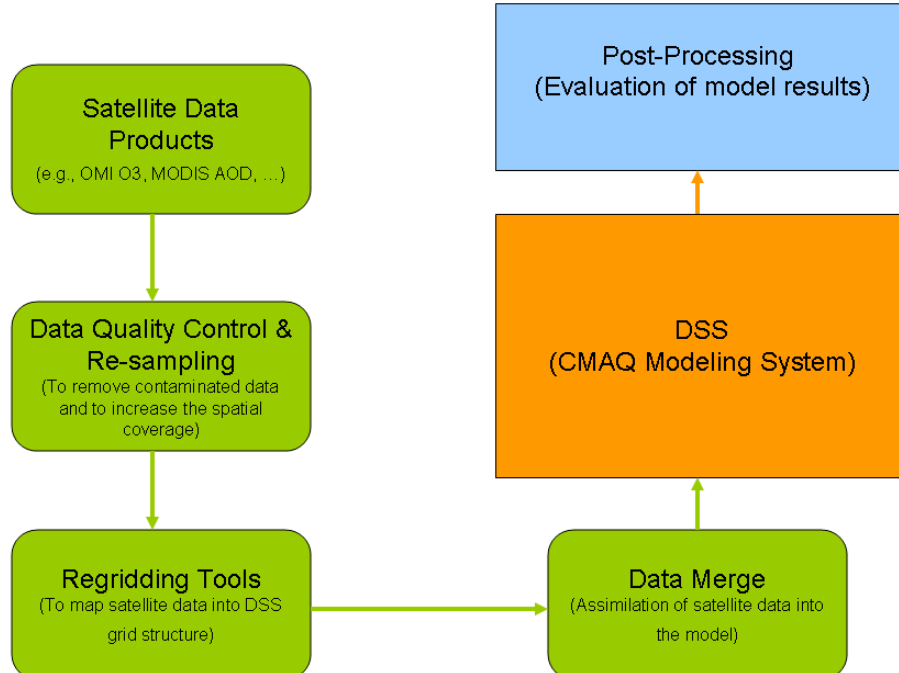


Figure 1- Flowchart representing the approach taken in merging the satellite data with model input data.

D. NASA Earth Science research products

We used the following NASA datasets to build initial and boundary conditions for the air quality model.

1. Ozone Monitoring Instrument (OMI) aboard the Aura satellite measures vertically-resolved concentration of Ozone (O₃), which has a nominal ground footprint of 13 x 48 km² at nadir. We achieve complete global coverage in one day. Dr. Xiong Liu at Goddard Earth Sciences and Technology Center (GEST) developed the data for this project.
2. MODIS- Moderate Resolution Imaging Spectroradiometer (MODIS) onboard Terra and Aqua satellites provide daily Aerosol Optical Depth (AOT). We have used Level 2 aerosol product, which has an approximate resolution of 10 km at nadir. This dataset is available from <http://ladsweb.nascom.nasa.gov/data/>.
3. RAQMS- Three-dimensional output from the Real-time Air Quality Modeling System (RAQMS), [R. B. Pierce, et al., 2003; R. B. Pierce, et al., 2007] builds O₃ boundary condition for CMAQ-CTM.

E. Description of the modeling experiment

1. General Overview

MM5, SMOKE, and CMAQ modeling systems conducted the modeling of atmospheric dynamics and chemistry observed during August 2006. We conducted the simulations on a 36-km resolution with a Lambert Conformal map projection and origin at 47 N and 90 W and true latitudes at 33 N and 45 N. It has 164 cells in the east-west and 148 cells in the north-south direction. 50 mb is the top of the modeling grid and 39 vertical layers of varying thickness. A set of four air-quality model simulations (Table 1) demonstrates improvement in air quality model predictions that can be achieved when satellite data and/or a global chemical transport model is used to provide lateral boundary condition for CMAQ. We compare the meteorological and air quality model performance to land-based observation stations (i.e., EPA surface monitors and NOAA ozonesondes).

Table 1- Description of four air-quality model simulations.

Name of the simulation	Description
CNTRL	A control simulation in which CMAQ is initialized only once at the beginning of the simulation and runs continuously for the entire simulation period using the standard boundary condition
SATBC	A simulation similar to control except that BC was constructed by merging satellite observations and model fields
SATICBC	A simulation similar to SAT_BC but re-initializing the model every 24 hours by assimilating satellite observations into the model fields
RAQMSBC	A simulation similar to the control but a continuous BC is constructed from Real-time Air Quality Modeling System (RAQMS) global model

2. Air quality modeling (CMAQ-CTM) configuration

CMAQ-CTM [Byun and Schere, 2006; Dennis, et al., 1996] version 4.6 contains state-of-the-science parameterization of atmospheric processes affecting transport, transformation, and deposition of pollutants such as ozone, particulate matter, airborne toxics, and acidic and nutrient pollutant species. It incorporates output fields from the meteorological (e.g., MM5) and emissions (e.g., SMOKE) modeling systems and several other data sources through special processors. The meteorological data is

processed using Meteorology Chemistry Interface Processor (MCIP) [Otte, et al., 2004], initial and boundary conditions through ICON and BCON and clear sky photolysis rate using JPROC. Initial and boundary condition processors allow the use of a gridded concentration field as well as the species concentration profiles, which are available with the installation. JPROC generates the photolysis rate reference table under clear sky conditions.

We used MCIP version 3.3 to create meteorological input files for CMAQ-CTM. Most meteorological variables pass through directly from the MM5 output fields. MCIP computed the others, such as dry deposition velocities. A set of predefined vertical profiles, which are available with the CMAQ installation, generate initial and boundary conditions for the 36-km domain. The processor JPROC generates the clear sky photolysis rates. We performed the process using modified extraterrestrial radiation data from the World Meteorological Organization (WMO) [Chang, et al., 1990] and O₂ and O₃ absorption cross-section data from NASA [DeMore, et al., 1994]. Table 2 shows the CMAQ-provided scientific options for various atmospheric processes (e.g., gas-phase chemistry, advection).

Table 2- Scientific options for various CMAQ-provided atmospheric processes.

Physical Process	Reference
Horizontal and vertical advection	YAMO
Horizontal diffusion	MULTISCALE
Vertical diffusion	ACM2
Gas-phase chemistry and solver	EBI_CB4
Gas and aqueous phase mechanism	CB4_AE3_AQ
Aerosol chemistry	AERO3
Dry deposition	AERO_DEPV2
Cloud dynamics	CLOUD_ACM

3. Meteorological modeling

We conducted the meteorological modeling for the study period using the fifth-Generation Penn State/NCAR Mesoscale Model (MM5) [Dudhia, 1989; Grell, et al., 1995]. Maintained by the National Center for Atmospheric Research (NCAR), MM5 is the last in a series of Mesoscale models first developed at Penn State in the early 1970's [Anthes and Warner, 1978]. Since that time, it has e to broaden its usage. These changes include: (1) a multiple-nest capability; (2) non-hydrostatic dynamics, which allow the model to be used at a few-kilometer scale; (3) multi-tasking capability on shared- and distributed-memory machines; (4) four-dimensional data-assimilation (FDDA) capability, and (5) multiple physics options. Meteorological field development for air quality modeling application uses this model extensively.

Like any other prognostic meteorological model, MM5 requires a significant amount of terrestrial (i.e., topography, Land Use/Land cover) and atmospheric data (e.g., gridded analysis fields, which include at a minimum sea-level pressure, wind, temperature, relative humidity, and observations that contain soundings and surface reports). This modeling project used the following datasets:

- a) Surface elevation, Land Use/Land Cover (LULC), soil type, and other terrestrial datasets from United States Geological Survey (USGS);
- b) NCEP ETA gridded-analysis data at 40-km resolution archived at 3-hour intervals available at <http://dss.ucar.edu/datasets/ds609.2>;
- c) Surface (land and ship) and upper air observational data archived at 3- and 6-hour intervals at available at <http://dss.ucar.edu/datasets/ds464.0>;
- d) Hourly surface observations for over 1,000 stations in U.S. and Canada available at <http://dss.ucar.edu/datasets/ds472.0>

We conducted modeling simulations using MM5 version 3.7 and performed data processing in six-day segments beginning July 1 and ending October 3. The NCEP ETA gridded-analyses data is first processed through the program PREGRID and mapped onto the 36-km via the REGRIDDER. The analyses fields with the help of the program LITTLE_R incorporate surface, ship, and upper air data. Finally, INTERPF interpolates pressure level fields generated by LITTLE_R onto MM5 sigma coordinates. We based the MM5 model configuration (Table 3) on a brief literature review of recent modeling projects in support of air quality management activities.

Table 3- MM5 Model Configuration.

Physics options	
Nesting Type	One-way
Numerical Time Step	90 sec
Cumulus parameterization	Grell
PBL scheme	MRF
Microphysics	Reisner 1
Radiation scheme	RRTM scheme
Land Surface scheme	Noah-LSM
Convection scheme	KF2
Observation nudging	None
3-D Grid analysis nudging	Yes
3-D Grid analysis nudging time interval	3-hour
3-D Grid analysis nudging co-efficient	$GU=2.5 \times 10^{-4}$, $GV=2.5 \times 10^{-4}$, $GT=2.5 \times 10^{-4}$, $GQ=1.0 \times 10^{-5}$
Surface Analysis nudging	Yes
Surface Analysis nudging time interval	3-hour
Surface Analysis nudging co-efficient	$GU=2.5 \times 10^{-4}$, $GV=2.5 \times 10^{-4}$

METSTAT software, developed by the ENVIRON corporation, evaluated the model performance (<http://www.camx.com/files/metstat.15feb05.tar.gz>). It computes surface statistics for temperature, wind speed and direction, and humidity. The metrics include: Bias Error (B), Gross Error (E) and Root Mean Square Error (RMSE), Systematic Root Mean Square Error (RMSEs), Unsystematic Root Mean Square Error (RMSEu) and Index Of Agreement (IOA). Table 4 shows the mathematical formulation of these variables.

Table 4- Metrics for evaluating meteorological model performance.

Metrics	Formulation
Bias	$B = \frac{1}{IJ} \sum_{j=1}^J \sum_{i=1}^I (P_j^i - O_j^i)$
Gross Error	$E = \frac{1}{IJ} \sum_{j=1}^J \sum_{i=1}^I P_j^i - O_j^i $
Root Mean Square Error	$RMSE = \left[\frac{1}{IJ} \sum_{j=1}^J \sum_{i=1}^I (P_j^i - O_j^i)^2 \right]^{1/2}$
Systematic Root Mean Square Error	$RMSE_S = \left[\frac{1}{IJ} \sum_{j=1}^J \sum_{i=1}^I (\hat{P}_j^i - O_j^i)^2 \right]^{1/2}$
Unsystematic Root Mean Square Error	$RMSE_u = \left[\frac{1}{IJ} \sum_{j=1}^J \sum_{i=1}^I (P_j^i - \hat{P}_j^i)^2 \right]^{1/2}$
Index of Agreement	$IOA = 1 - \left[\frac{IJ \cdot RMSE^2}{\sum_{j=1}^J \sum_{i=1}^I P_j^i - M_o + O_j^i - M_o } \right]$

Table 6 illustrates the monthly average performance statistics for August 2006. In an effort to identify model biases and error over different regions of the domain, we have computed statistics for sub-regions shown in Figure 2. The results of the statistical analysis show that the simulation captures meteorological conditions observed during the study period with the adequate level of accuracy. Performance statistics for most days are within [Emery, et al., 2001]’s proposed benchmarks (Table 5).

Table 5- Emery’s (2001) proposed benchmarks.

Statistical Measure	Benchmark
Wind Speed Bias (m/s)	<±0.5
Wind Speed Total RMSE (m/s)	2.0
Wind Speed Index of Agreement	0.6
Wind Direction Gross Error (degree)	30.0
Wind Direction Bias (degree)	<±10.0
Temperature Bias (Kelvin)	<±0.5
Temperature Gross Error (degree)	2.0
Temperature Index of Agreement	0.8
Humidity Bias (g/kg)	<±1.0
Humidity Gross Error (g/kg)	2.0
Humidity Index of Agreement	0.6

To examine whether the simulation could capture large-scale synoptic features, we compared the modeling results against weather charts from UNISYS web site [http://weather.unisys.com/]. Figure 3 shows weather charts for July 15 alongside MM5 result. The model wind speed, direction, and temperature are in reasonable agreement with observations. The model is able adequately captures the

stationary front, which passed through Dallas Fort Worth on August 21 and 22. The slow-moving system extended all the way to east coast and was associated with high ozone episode and sporadic cloudiness.

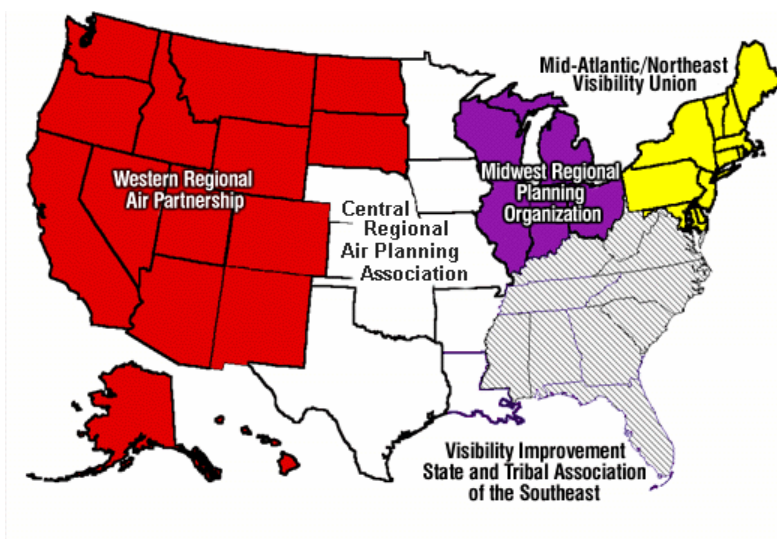


Figure 2- Five sub-regions for surface evaluation.

Table 6- Monthly average performance statistics of meteorological simulations for August 2006.

			CENRAP	MANEVU	MWRPO	VISTAS	WRAP
Wind Speed	Mean OBS	(m/s)	2.97	2.70	2.49	2.05	3.24
Wind Speed	Mean PRD	(m/s)	2.47	2.35	2.41	1.94	2.43
Wind Speed	Bias	(m/s)	-0.50	-0.35	-0.09	-0.11	-0.81
Wind Speed	Gross Error	(m/s)	1.26	1.48	1.17	1.21	1.64
Wind Speed	RMSE	(m/s)	1.65	2.03	1.50	1.54	2.11
Wind Speed	Sys RMSE	(m/s)	1.35	1.67	1.14	1.24	1.81
Wind Speed	Unsys RMSE	(m/s)	0.94	1.13	0.97	0.91	1.09
Wind Speed	IOA		0.73	0.59	0.70	0.68	0.66
Wind Direction	Mean OBS	(deg)	149.90	189.95	167.60	160.32	255.55
Wind Direction	Mean PRD	(deg)	151.30	203.67	171.11	164.80	246.42
Wind Direction	Bias	(deg)	2.77	4.91	4.53	4.84	6.16
Wind Direction	Gross Error	(deg)	25.72	27.81	24.58	33.14	43.26
Temperature	Mean OBS	(K)	298.38	294.37	294.96	299.75	294.38
Temperature	Mean PRD	(K)	298.61	293.58	294.47	300.10	294.01
Temperature	Bias	(K)	0.23	-0.79	-0.50	0.35	-0.38
Temperature	Gross Error	(K)	2.08	2.09	2.08	2.11	2.99
Temperature	RMSE	(K)	2.81	2.70	2.68	2.85	3.87
Temperature	Sys RMSE	(K)	1.02	0.85	0.82	0.99	0.54
Temperature	Unsys RMSE	(K)	2.60	2.53	2.53	2.66	3.82
Temperature	IOA		0.95	0.92	0.91	0.90	0.93
Humidity	Mean OBS	(g/kg)	14.38	11.54	12.71	16.37	8.13
Humidity	Mean PRD	(g/kg)	13.24	11.21	11.91	15.23	7.21
Humidity	Bias	(g/kg)	-1.13	-0.33	-0.81	-1.14	-0.92
Humidity	Gross Error	(g/kg)	1.64	1.12	1.42	1.71	1.53
Humidity	RMSE	(g/kg)	2.08	1.44	1.77	2.17	2.03
Humidity	Sys RMSE	(g/kg)	1.23	0.69	1.10	1.28	1.32
Humidity	Unsys RMSE	(g/kg)	1.64	1.23	1.35	1.73	1.53
Humidity	IOA		0.86	0.84	0.79	0.76	0.86

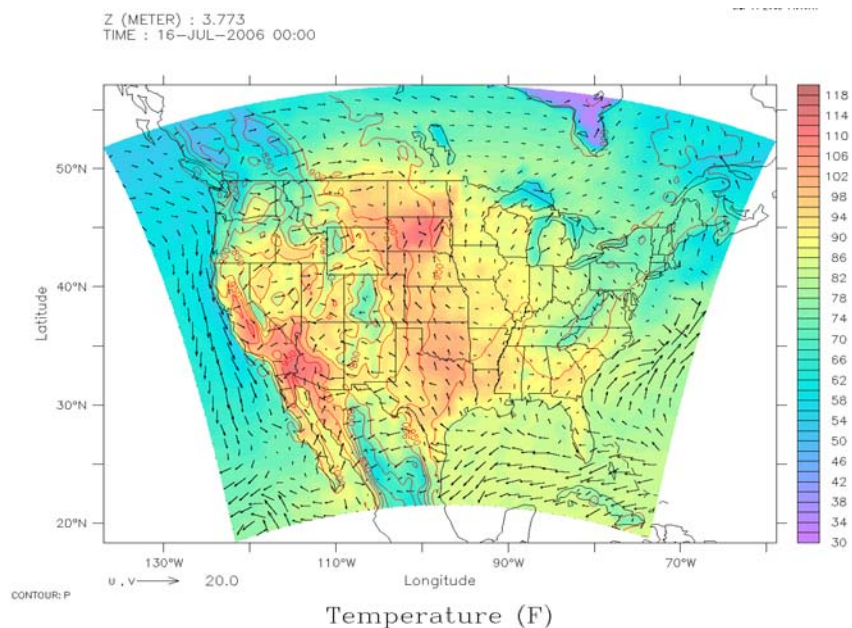
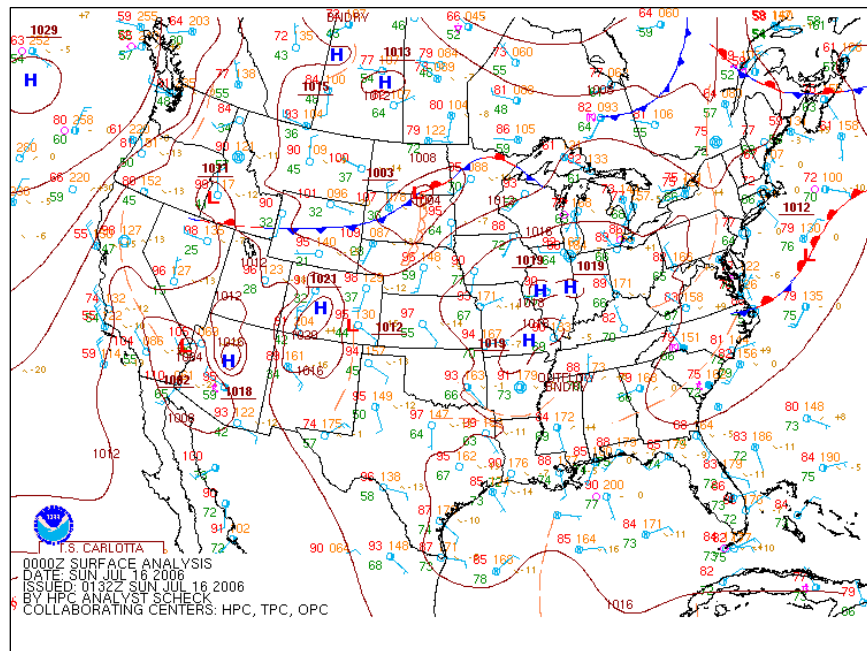


Figure 3- Weather charts for July 15 alongside MM5 result. The model wind speed, direction, and temperature are in reasonable agreement with observations.

4. Emissions processing

Emission inventories are typically available with an annual or daily total emissions value for individual emissions sources or source categories. Since air quality models require emissions data on an hourly basis for each model grid-cell and species, emission processors convert the available emissions data into a form the air quality model can ingest. The Sparse Matrix Operator Kernel Emissions (SMOKE) processor [Coats, 1996; Houyoux, et al., 2000] is one particular tool, and it created gridded, temporalized,

and speciated emission files for this project. SMOKE is capable of generating temperature-sensitive mobile source emission factors using EPA's MOBILE6 emission factors model. It is also capable of generating biogenic emissions for this research work with the help of Biogenic Emissions Inventory System (BEIS) version 3.09 [Guenther, et al., 2000; T. Pierce, et al., 1998]. In addition to large amounts of source-specific data, certain aspects of emissions processing require meteorological variables. The meteorological model provided the variables and included daily surface temperature for calculating mobile source emission factors; temperature and radiation fields for calculating biogenic emissions; and Planetary Boundary Layer (PBL) height, surface heat flux, wind speed, and temperature for estimating plume rise for point sources.

In the absence of any consolidated annual emissions inventory for 2006, we are using the 2002 Annual Emission Inventory developed by Regional Planning Organizations (RPOs) in response to regulatory requirements established under the Regional Haze Rule (RHR). We are accounting for on-road mobile source emissions reductions; however, these reductions will likely change due to fleet turnover. We are also using the 2006 Continuous Emissions Monitoring (CEM) data for Electricity Generating Units (EGUs) compiled by EPA's Clean Air Markets Division (CAMD). Given the overall uncertainty in emission estimates, determining the emission reduction in two major source categories provides us with a reasonable estimate of emissions for this research work. Table 7 illustrates the daily average emission totals and spatial plots of NO_x, VOC, total Carbon, SO₂, NH₃, and CO.

Table 7- Domain-wide daily emission totals in tons per day.

	NOX	VOC	CARBON	SO2	NH3	CO
Area	3308.18	12604.77	1212.27	2550.13	6933.41	12066.45
EGU	10387.81	147.68	78.99	30651.54	46.21	2095.20
Mobile	14935.43	8801.20	214.07	329.87	0.00	99360.72
Non-EGU	12904.17	3100.11	347.01	18215.97	633.57	10320.65
Non-road	12242.84	9819.18	919.69	1248.35	12.38	87420.60

5. Pre-processing of satellite/ozonesonde data

5a. Processing of ozonesonde and OMI satellite observations for CMAQ-CTM

The Ozone Monitoring Instrument (OMI) on the Aura satellite measures the total columns of O₃ with a nominal ground footprint of 13x48 km² at nadir. Essentially, we achieve complete global coverage in one day. 270-330 nm OMI radiances (currently an off-line data product) (Liu et al., 2005) deliver O₃ concentrations at 24 ~2.5-km thick layers from surface to ~60 km. Instrumental calibration error and inadequate forward modeling (e.g., aerosols, clouds) significantly reduce the information retrieved in the lower troposphere.

A "drop-in-box" method resamples daily OMI O₃ measurements onto the 36-km equal area CMAQ-CTM grid. CMAQ-CTM grids with center points that fall within this specific OMI pixel assign the OMI O₃ value. A CMAQ grid that receives more than one OMI O₃ value applies a simple average to get a mean value. The original OMI O₃ data set has already filtered out some unreasonable values, and we have not applied any further filtering criteria yet. The nearest neighbor re-sampling algorithm fills in data that might have been lost due to cloud contamination. Finally, OMI O₃ profiles, available at constant pressure surfaces, vertically interpolate onto the 39 sigma-P pressure layers of CMAQ-CTM model. Figure 4 illustrates this process in the horizontal domain, and Figure 5 illustrates the vertical dimension.

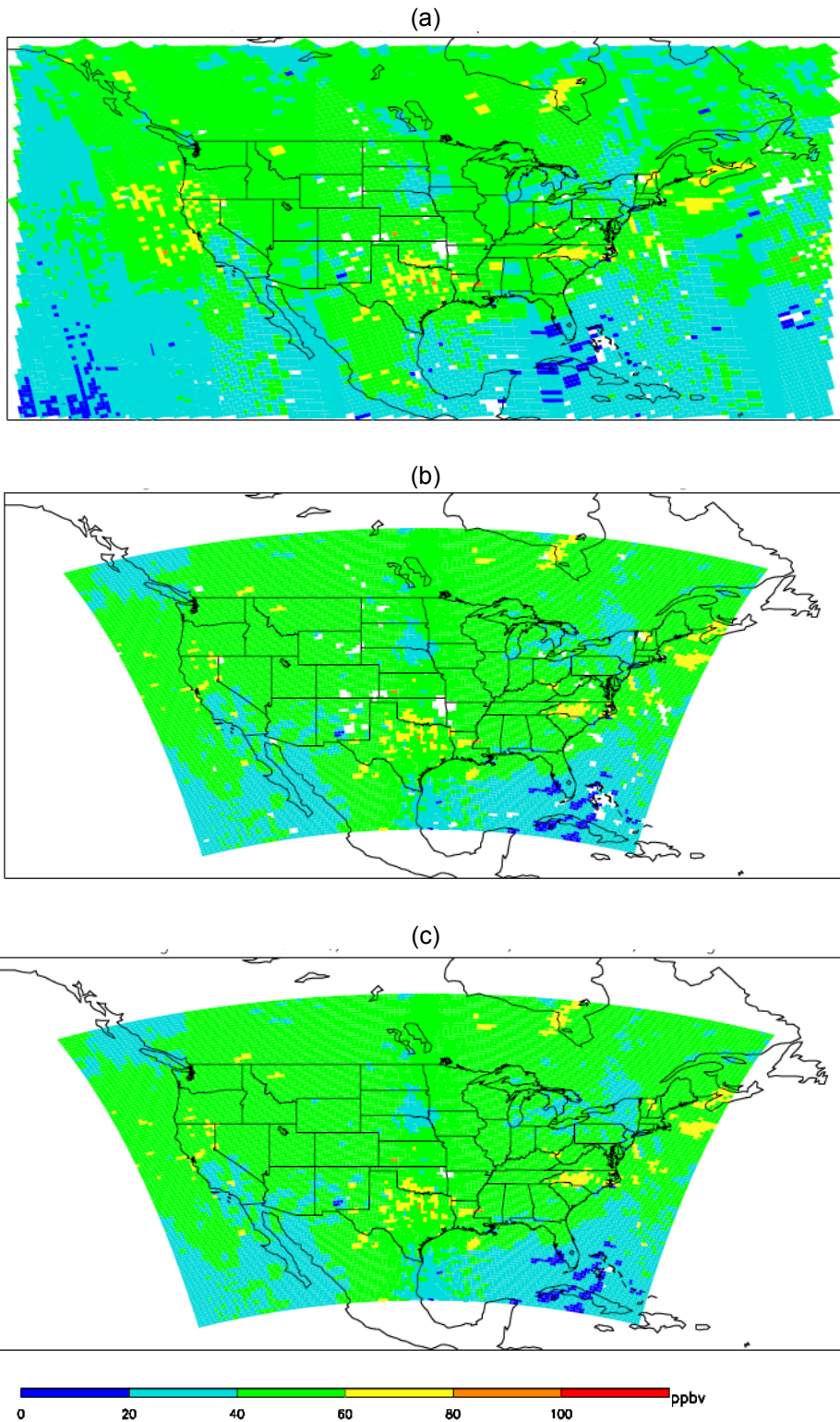


Figure 4- (a) AURA OMI/O₃ observations at the first OMI layer (1013-701mb) orbits over continental U.S., August 21, 2006. (b) OMI/O₃ observations are resampled to CMAQ-CTM grids. (c) Nearest neighbor re-sampling algorithm is then applied to fill-in data that might have been lost due to cloud contamination.

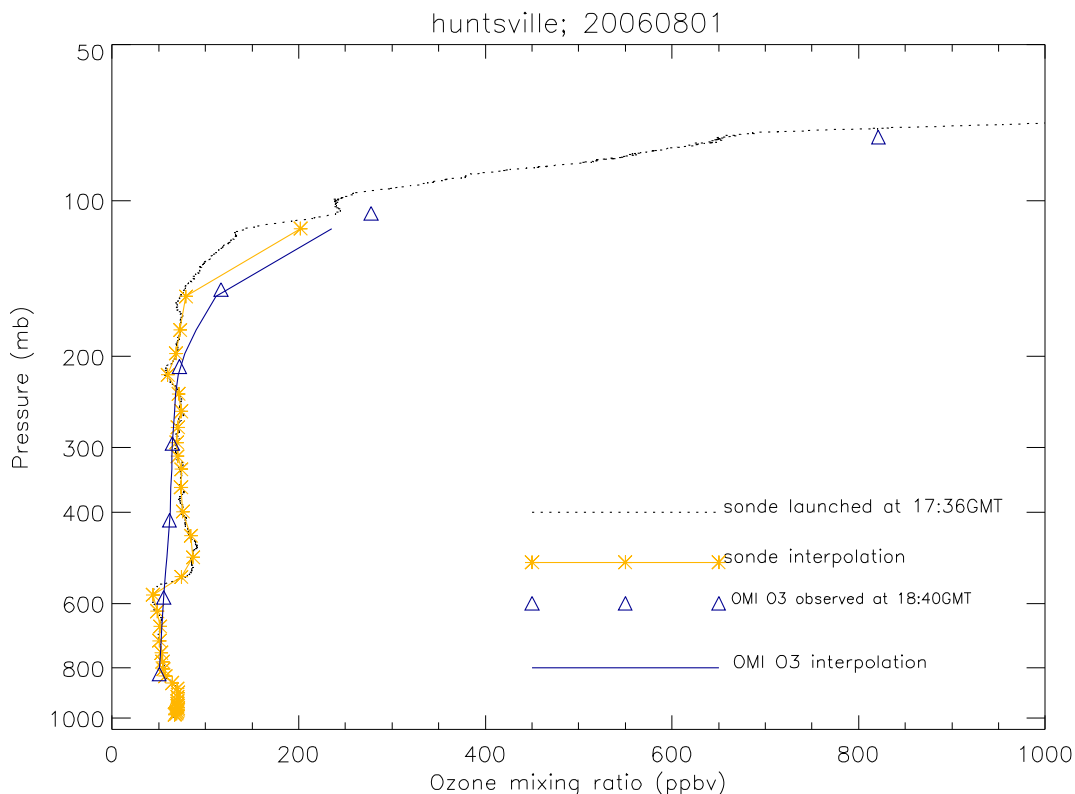


Figure 5- An example of re-sampling ozonesonde and OMI/O₃ profiles onto CMAQ vertical layers at Huntsville, AL, August 1, 2006.

5b. Processing of Aerosol Optical Depth (AOT) from MODIS

Particulate Matter (PM) is one of the important factors included in the determination of air quality. Realistic representation of emission, transport, and removal of particulate matter is essential in air quality studies. Air quality models require datasets for initializing and specifying the lateral boundary conditions in the case of limited area models. Ground observations provide routine observations of PM but have limited spatial coverage. Multi-channel satellite imagery furnishes the column burden of atmospheric aerosols. Satellite-retrieved aerosol optical depth (AOD) and mean particle size are available at spatial resolutions that are adequate for use in air quality models. While the total column AOD from the satellite provides the spatial distribution of aerosol burden, the vertical distribution of aerosols assists in utilizing such data in air quality models. However, only few satellite sensors provide vertical distribution of atmospheric aerosols on a limited spatial coverage (e.g., the Cloud-Aerosol Lidar and Infrared Pathfinder Satellite Observation, CALIPSO). In this project, we examine a technique for utilizing Moderate Resolution Imaging Spectroradiometer (MODIS)-retrieved aerosol optical depths in CMAQ, which is a widely used air quality model. The technique uses CMAQ-predicted vertical distribution of aerosols as the template for distributing satellite-derived AOT into atmospheric columns in CMAQ and assumes that the spatial distribution of emission sources are reasonably defined in the model, and the model performs reasonably well with respect to vertical mixing. Therefore, the discrepancies between the model AOD and the observed AOD are due to either emission source strength or the representation of aerosol chemistry/formation in the model. This project quantifies enhancement to air quality predictions derived through applying satellite-observed aerosol fields to the CMAQ model.

MODIS is an instrument aboard the [Terra \(EOS AM\)](#) and [Aqua \(EOS PM\)](#) satellites, both in a sun-synchronous orbit. Terra's orbit around the Earth is timed, so it passes from north to south across the equator in the morning (about 10:30 AM local time), while Aqua passes south to north over the equator in

the afternoon (about 1:30 PM local time). MODIS views the entire Earth's surface every 1 to 2 days, acquiring data in 36 spectral bands. This project utilizes daily aerosol optical thickness (AOT, hereafter used interchangeably with AOD) retrieved from imagery captured by MODIS sensors on both platforms. The time period considered is August 2006. Since TERRA-MODIS acquires imagery during the morning (10:30 AM) and AQUA-MODIS in the afternoon (1:30 PM), combined aerosol fields retrieved from both Terra and Aqua MODIS imagery can create a more complete dataset for use in CMAQ. The rationale for combining the data are: 1) MODIS sensor takes approximately four hours to image the entire region covered by the Continental United States (CONUS), and it is not possible to obtain simultaneous aerosol observations; 2) Aerosol retrievals are not available when cloud cover is present; thus, combining aerosol retrievals from the two platforms, increase the probability of obtaining a successful retrieval at a given location. The latter is especially true in case of partly cloudy scenes and/or presence of short-lived clouds.

Spatial resolution of MODIS level 2 aerosol product is 10 km by 10 km at nadir, which is resampled to the 36-km x 36-km resolution equal area grid utilized by the CMAQ model. Note that the MODIS-observed AOD, resampled to CMAQ grid, initializes and provides lateral boundary conditions for CMAQ. In addition, this data is comparable to the CMAQ-predicted aerosol fields. Since the MODIS AOD is a combination of observations from both Terra and Aqua platforms, it is compared against CMAQ-simulated AOD averaged over a period (1500-2200 UTC), which is consistent with daytime observation window for Terra and Aqua platforms over CONUS region.

Even after combining aerosol fields from Terra and Aqua, one of the difficulties encountered in creating AOD fields was missing retrievals due to presence of clouds. In order to obtain a smoothed AOD field, we devised a nearest neighbor resampling approach. If a missing value of AOD exists in combined Terra-Aqua product (before resampling to CMAQ grid), the algorithm must find a three-pixel radius neighborhood for a valid AOD observation. For valid observations, the average of neighboring pixels replaces the missing value. Sensitivity studies of this process to the radius of the search neighborhood show a three-pixel radius is adequate. Table 8 shows the results for a case study in August 14, 2007. While going away from a missing pixel reduces the number of missing data, it also increases the uncertainty of the value assigned to the missing pixel.

The procedure fills in the majority of the missing data pixels in the region and creates a smoothed AOD field. In order to examine the validity of the resampling procedure, we conducted the following experiment.

Figure 6 illustrates another example of pixel extension algorithm described above for September 7, 2006. From the original Terra-Aqua-combined MODIS AOD image (Figure 6a), 50 % of the non-zero AOD was randomly removed (Figure 6b). In successive attempts, we extended the coverage by increasing the radius of search from 1-pixel to 3-pixels. 1-pixel extension recovered 57 % of the removed data, while 2- and 3-pixel extensions recovered 73 % and 82 % of the removed data, respectively. The correlation coefficient between the recovered data and the original data remains relatively unchanged (.88) indicating that even going out by 3 pixels for the search does not increase the error in the recovered data significantly, while it increases the number of recovered data considerably. We applied the scatterplot between the original AOD values of the randomly removed pixels and the values obtained for the same locations after the resampling procedure to the modified field to show that the majority of the points cluster along the one-to-one line. We performed the same experiment on the August 14, 2007 case, and it resulted in a correlation coefficient of .93 suggesting a good agreement between the original AOD field and the recovered data.

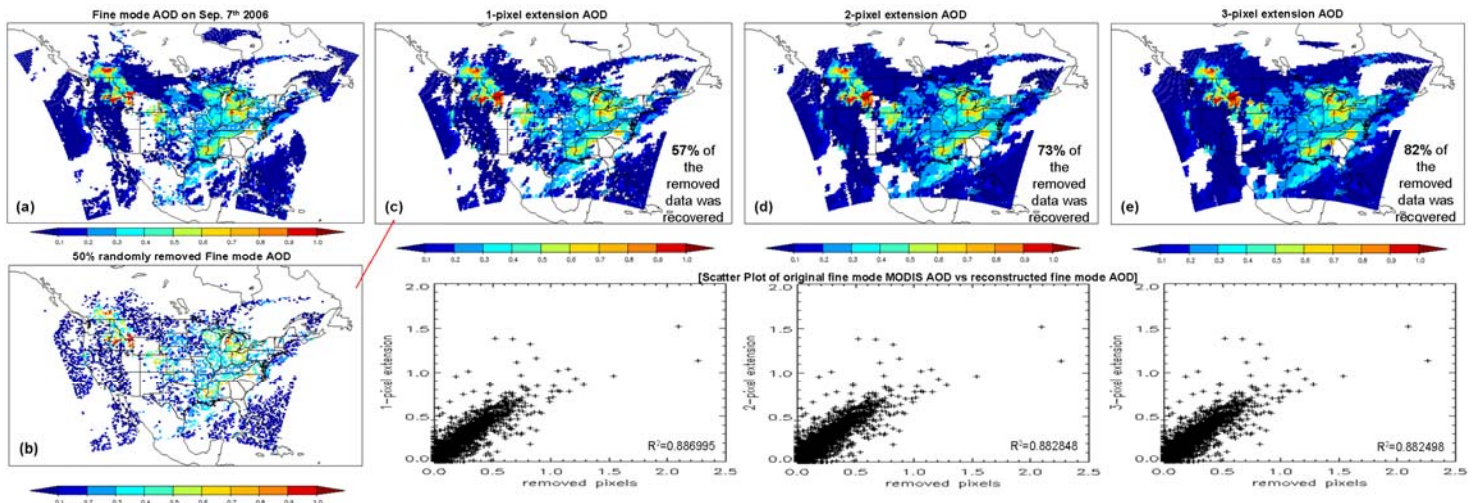


Figure 6- Pixel Extension Algorithm (PEA) allows for increasing MODIS coverage by reconstructing missing values due to cloud contamination. (a) MODIS AOD from TERRA and AQUA on September 7, 2006. (b) We randomly removed 50 % pixels from original image (a). (c, d, e) Reconstructed image using 1, 2, and 3 pixel extension.

Table 8 - The percentage of missing pixels within MM5 area.

	08/01	08/02	08/03
2 pixels	31.5 %	34 %	34 %
3 pixels	18 %	20.7 %	21.8 %
4 pixels	10 %	13 %	14 %

We needed information obtained from CMAQ regarding vertical distribution of aerosols for effective use of MODIS AOD in the model. The dependency of the technique to the information from the model implies that the aerosol module used has a decisive impact on the aerosol speciation and distribution. In this exercise, we used the standard aerosol module in CMAQ as described in [Binkowski and Roselle, 2003] with updates described in [Bhave, et al., 2004]. The aerosol distribution is modeled as a superposition of three lognormal modes that nominally correspond to Aitken (particles with diameter < .1 μm), accumulation (particles with 0.1 < diameter < 2.5 μm), and coarse (particles with diameter > 2.5 μm) modes. In the current exercise, we use two aerosol categories, fine, and coarse modes. Fine mode consists of aerosols with aerodynamic diameter of less than 2.5 micrometers (PM_{2.5}), while coarse mode consists of aerosols with diameter greater than 2.5 micrometers. The sum of the species concentrations over the Aitken and accumulation modes determines the model results for PM_{2.5} concentrations. Table 9 shows CMAQ aerosol species (as represented in CMAQ aerosol module). The fine mode aerosol species comprise sulfate, nitrate, ammonium, anthropogenic and biogenic organic carbon, elemental carbon, and other unspecified species originating from human activity.

MODIS level 2 data provides fine mode fraction, which is the fractional contribution of fine mode to total AOD. We used fine mode fraction data in this project to separate out fine and coarse mode AOD. However, fractional contributions made by the different aerosol species to fine and coarse mode aerosols and knowledge of vertical distribution is necessary to utilize MODIS AOD. The following statements provide closure: 1) The CMAQ-simulated profile for the corresponding time gives the vertical distribution of different aerosol species; 2) The percentage contribution of an aerosol species to the total particulate mass within a column is the same as that obtained from CMAQ simulations for the corresponding time. Based on these assumptions, the following ratio parameter (α) scales the aerosol mass concentration in a CMAQ vertical column:

$$\alpha = \frac{\tau_{MODIS}}{\tau_{CMAQ}}$$

Where τ_{MODIS} and τ_{CMAQ} are MODIS and CMAQ aerosol optical depths (AOD), respectively. For the model, τ_{CMAQ} becomes:

$$\tau_{CMAQ} = \int_0^{Z_{top}} B_{ext} dz$$

Where B_{ext} is the aerosol extinction coefficient (km^{-1}), and Z is the height in km. To arrive at aerosol extinction coefficient, we used an empirical relationship devised from long-term measurements at the Interagency Monitoring of Protected Visual Environments (IMPROVE) sites [Hand and Malm, 2005], including the new revisions made based on the current information (http://vista.cira.colostate.edu/improve/Publications/GrayLit/019_RevisedIMPROVEeq/RevisedIMPROVEAlgorithm3.doc). The extinction coefficient (Mm^{-1}) is calculated as:

$$\begin{aligned} \beta_{ext} \approx & 2.2 \times f_s(rh) \times [\text{Small Sulfate}] + 4.8 \times f_L(rh) \times [\text{Large Sulfate}] \\ & + 2.4 \times f_s(rh) \times [\text{Small Nitrate}] + 5.1 \times f_L(rh) \times [\text{Large Nitrate}] \\ & + 2.8 \times [\text{Small Organic Mass}] + 6.1 \times [\text{Large Organic Mass}] \\ & + 10 \times [\text{Elemental Carbon}] + 1 \times [\text{Fine Soil}] + 1.7 \times f_{SS}(rh) \times [\text{Sea Salt}] \\ & + .6 \times [\text{Coarse Mass}] + 1 \times [\text{Rayleigh Scattering (Site Specific)}] + .33 \times [\text{NO}_2 \text{ (ppb)}] \end{aligned}$$

The algorithm uses three water-growth adjustment terms. The small size distribution (S) and the large size distribution (L) of sulfate and nitrate compounds and for sea salt ($f_s(RH)$, $f_L(RH)$ and $f_{SS}(RH)$, respectively) use the adjustment terms. The elevation and annual average temperature of each of the IMPROVE monitoring sites includes site-specific Rayleigh scattering calculations.

Hourly-modeled AOD averages to corresponding MODIS tracking time, which is from 15 to 22 GMT to obtain the ratio α . In order to eliminate the site-specific impact of Rayleigh scattering ($\int (\text{Rayleigh_scattering}) dz$), the adjustment is applied only if the MODIS AOD (τ_{MODIS}) is greater than Rayleigh scattering. Thus, when the impact of Rayleigh scattering is greater than zero, the ratio becomes:

$$\alpha = \frac{\left\{ \tau_{MODIS} - \int (\text{Rayleigh_scattering}) dz \right\}}{\int (\beta_{ext} - \text{Rayleigh_scattering}) dz}$$

If Rayleigh-scattering impact does not exist and MODIS data are available, then the ratio becomes:

$$\alpha = \frac{\tau_{MODIS}}{\int \beta_{ext} dz}$$

Note that assumption is the difference between satellite data, and model data of AOT is only for mass-scaling discrepancy. Another assumption is a revised new IMPROVE equation, which is explained to AOT from CMAQ model. The algorithm applies the ratio calculated above to each aerosol mass concentration in each layer. All 16 fine aerosol species in Table 9 (I and J modes, except water) are scaled by α . Also, note that while NO_2 is used in IMPROVE equation for calculating the aerosol extinction coefficient, it will not be scaled by α . Figure 7 shows examples of scaled vertical profiles obtained using this procedure. When the value of α is less than 1, it reduces the mass concentration throughout the vertical column,

while values of α greater than 1 lead to an increase throughout the column. In cases where satellite-derived AOD is not available, the algorithm uses model calculations in place of the scaling procedures. For initial condition, we use satellite data of previous day (backward method), and for boundary condition, we use satellite data of next day (forward method).

Table 9- Speciation and variable name used in the CMAQ aerosol module.

Species description	Name
Aitken mode sulfate mass	ASO4I
Accumulation mode sulfate mass	ASO4J
Aitken mode ammonium mass	ANH4I
Accumulation mode ammonium mass	ANH4J
Aitken mode nitrate mass	ANO3I
Accumulation mode nitrate mass	ANO3J
Aitken mode anthropogenic secondary organic mass	AORGAI
Accumulation mode anthropogenic secondary organic mass	AORGAJ
Aitken mode primary organic mass	AORGPAI
Accumulation mode primary organic mass	AORGPAJ
Aitken mode secondary biogenic organic mass	AORGBI
Accumulation mode secondary biogenic organic mass	AORGBJ
Aitken mode elemental carbon mass	ACEI
Accumulation mode elemental carbon mass	ACEJ
Aitken mode unspecified anthropogenic mass	A25I
Accumulation mode unspecified anthropogenic mass	A25J
Aitken mode water mass	AH2OI
Accumulation mode water mass	AH2OJ

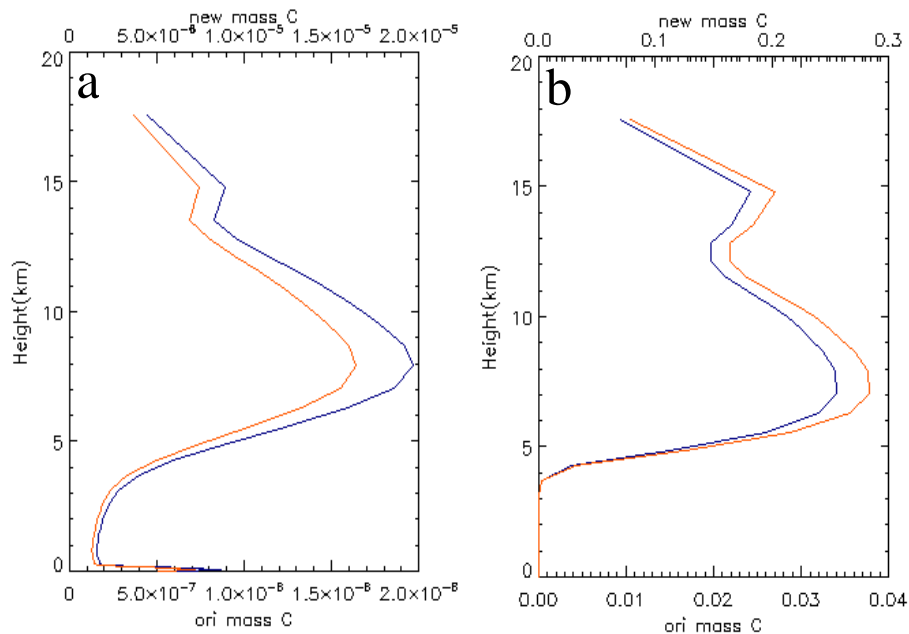


Figure 7- Vertical profiles of CMAQ mass concentrations scaled using the α parameter. a) Black carbon and, b) anthropogenic organic mass. Blue and red lines are the original CMAQ and scaled concentrations, respectively. Note that α parameter is less than 1.0 for the case shown in panel (a) and more than one for that shown panel (b).

5c. Processing of global model data for CMAQ-CTM

Another approach for providing IC and BC for CMAQ simulations would be using a global model that extends far beyond the regional modeling domain and could potentially illustrate the impact of long-range transport and recirculation outside the regional boundary. To establish a secondary reference point for evaluating the impact of direct use of satellite observations in this project, we constructed a continuous BC record from RAQMS global model predictions. Our collaborator in this project, Dr. Daewon Byun (formerly at University of Houston and currently with NOAA/ARL), provided the BCs for these simulations.

Data assimilation of OMI ozone column with NOAA GFS Global meteorology and the satellite fire detection data from MODIS Rapid Response produced the RAQMS data at 2-degree-by-2-degree resolution. The details on model configuration and emissions data used for the RAQMS simulations are summarized in [Al-Saadi, *et al.*, 2008]. It used emissions of CO, NO_x, and hydrocarbons estimated from the gridded carbon fuel consumption databases, satellite fire detections, and meteorology-based estimates of fire weather severity to estimate the amount of carbon released from active fires and ecosystem-dependent emission ratios.

Since we used previous spin-up simulations as the CMAQ IC inputs, we did not prepare any special IC files for CMAQ simulations from RAQMS outputs. The University of Houston, Institute for Multidimensional Air Quality Studies (IMAQS), developed the RAQMS2CMAQ conversion code, which constructed the BC files. The code initially processed RAQMS data for the 1999 simulations, and it originally required daily METCRO3D files for providing the pressure height information used in the vertical interpolation. For this project, we utilized a reference pressure-height coordinate instead. Additionally, since the recent version of MCIP did not provide all the necessary inputs for the conversion code, we modified the code to accommodate the limited information. A one-day BC file from control simulation set up the same species list in the BC file and verified the results of the new code with those from the original code for that one day. The interpolation with the fixed pressure levels may potentially be less precise than the MM5-provided dynamic pressure levels. On the other hand, interpolating with the fixed pressure levels may be more robust than utilizing the MM5 pressure levels, which are affected by the synoptic and local scale pressure perturbations.

We produced and verified a BC file after completion of the code modification. We compared the results with the University of Houston's (UH) 23-layer MM5 simulation case. Surprisingly, the ozone concentrations at the top level (39th layer) for the current case was substantially lower than those from the UH's top level (23rd layer) ozone. This difference could be due to the vertical resolution of the current model configuration in which the top layer is too thick to represent the stratospheric-tropospheric exchange processes. In the current model configuration, the top layer is very thick in order to have high vertical resolution around 10 km altitude. We used this configuration to minimize the artificial numerical mixing of high stratospheric ozone into the upper troposphere (through numerical diffusion).

The final sets of simulations investigate the efficacy of using satellite observations of ozone and aerosols to provide IC and BC for regional air quality simulations. It comprises two sets of simulations. The first sets of simulations, called SAT_BC, are similar to control except for the BC data they use. In SAT_BC simulations, we merged OMI ozone profiles and MODIS AOD with model predictions to construct daily BC files. The simulations perform in 24-hour segments, starting at 0:00 GMT, but the output from the previous segment, continuously initializes each new segment. In SAT_ICBC simulations, merging the satellite data with model predictions provide both BC and IC for each segment.

Satellite observations for the current day, used in conjunction with the current day simulation, prepare BC for these simulations. This combination is necessary due to the time offset between the observations and the model predictions. Combining the data from all the satellite tracks within a day, which span over several hours, while representing the same local time (about 1:30 PM) for any location, results in complete spatial coverage over the continental U.S. (CONUS). Furthermore, we are assuming that this single measurement can explain ozone and aerosol burden at lateral boundaries for a 24-hour simulation.

Since each segment starts at 0:00 GMT, the current day observations would be a better representation of the air outside the boundary. However, this technique is only applicable to retrospective modeling, such as regulatory air quality applications, where the current day observations are available.

BC only impacts the interior of the domain if the flow field is transporting air from outside the domain to the interior. Thus, the technique used in these simulations is not adequate for the situations where a strong flow field toward the domain and an observed transient event at the boundary exist. Future refinements to our technique will address this shortcoming as we plan to introduce diurnal variation for BC by projecting the observations away from the boundary to arrive at the boundary conditions for each given time.

In preparing IC files, the algorithm selects satellite observations from the previous day, because they are closer to the model initialization time of 0:00 GMT. Extracting concentrations from IC files at model grids that reside at the boundary simply constructs BC.

Figures 8 to 13 show the BC plots for O₃, PAN, HCHO, NO_x, CO and sulfate aerosol for south, east, north, and western boundaries for August 1, 2006. Each panel shows BC for control, RAQMS_BC, SAT_BC, and SAT_ICBC. The boundary conditions for SAT_BC and SAT_ICBC are identical due to the application of the same technique. The presented results emphasize the similarity. Figure 8 shows that both RAQMS_BC and SAT_BC ozone concentrations are significantly different from the control. In addition, both the satellite observation and RAQMS agree while OMI profiles indicate more stratospheric O₃ incursion into the mid-troposphere. Also of interest is the disagreement between the model and the satellite measurements in the western boundary where RAQMS indicates elevated O₃ concentrations in mid-troposphere that are not seen in the satellite observations. The figures also point to another limitation for the satellite data within the daytime boundary layer (below 1-km). The sharp vertical gradient around 1-km is because when OMI data is not available, we revert to the model value. Thus, the sharp gradient is demonstrating the contrast between higher OMI concentrations above 1 km and lower model values below this elevation.

Figure 9 shows similar plots for peroxyacetyl nitrate (PAN). Our technique extracts the BC from a modified IC file. CMAQ output at the end of the run for the previous 24-hour segment creates the IC file. Therefore, the emissions and the dynamics of the previous day consequently affect the IC and BC. This method explains the difference between BC for control and SAT_BC simulations. Interestingly, vertical distribution of PAN for SAT_BC shows remarkable agreement with RAQMS_BC. To a lesser degree, this resemblance in pattern is also manifested in formaldehyde distribution in Figure 10, meaning that the chemical evolution within the domain of study is mainly responsible for the overall characteristics of the air mass in the boundary as the regional model produces a similar distribution in PAN and formaldehyde as the global model predicts. Figure 11 illustrates such general agreement for NO_x on the eastern boundary while carbon monoxide does not exhibit a good agreement (Figure 12).

Figure 13 shows BC for sulfate aerosol (ASO₄). RAQMS did not extract this information and as evident from the figure, BC for RAQMS_BC is identical to the control simulation. However, since SAT_BC simulation extracts this information from the interior of the domain, the southern and eastern boundary experience the impact of ASO₄ loading.

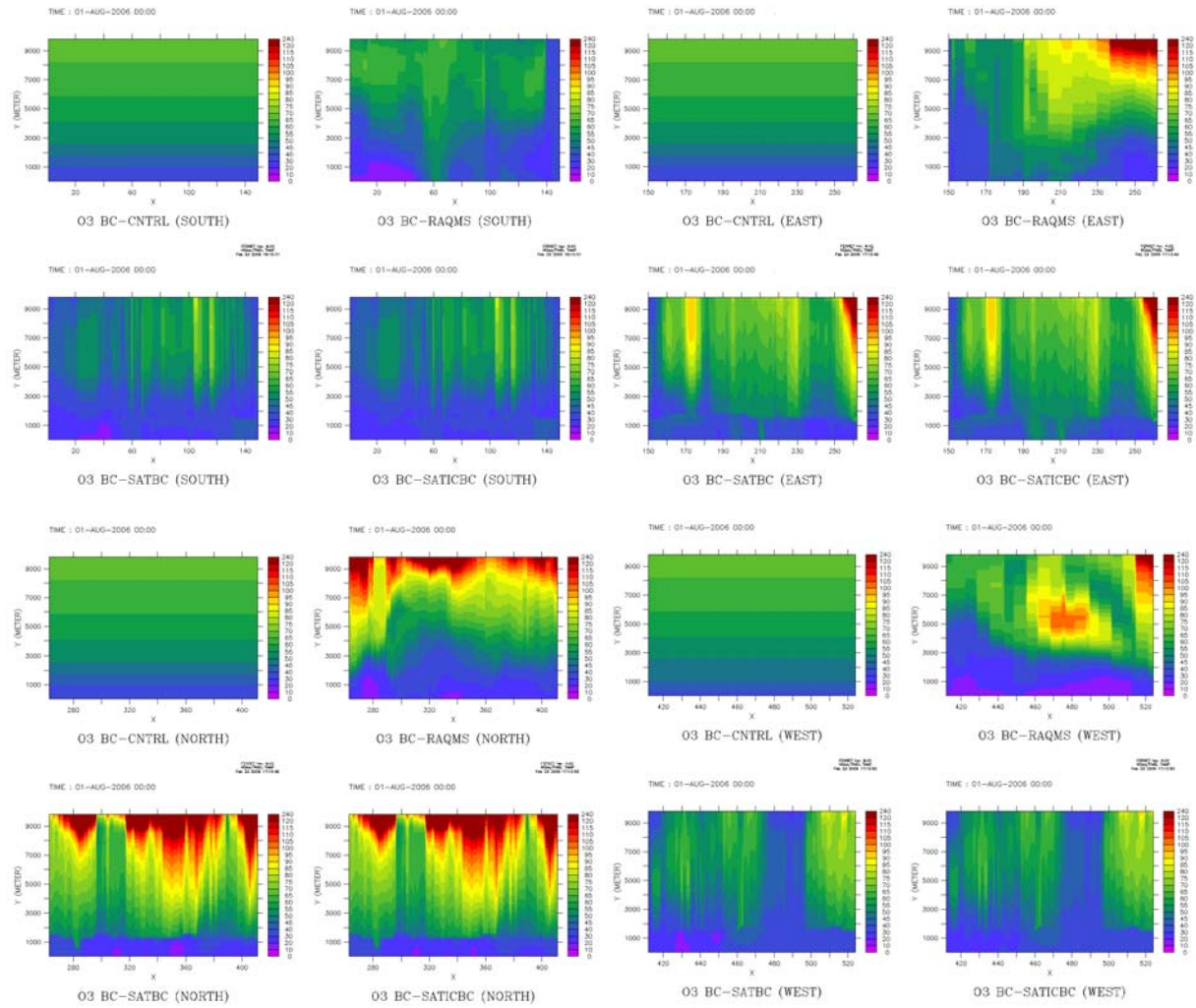


Figure 8– Ozone (ppb) BC for south, east, north, and west boundaries. In each panel, BC for control (top left, standard CMAQ BC), RAQMS_BC (top right, BC from RAQMS global model), SAT_BC (lower left, BC from satellite observations) and SAT_ICBC (lower right) simulations for August 1, 2006 are presented. Note that BC for SAT_BC and SAT_ICBC are identical. They are both included for completeness.

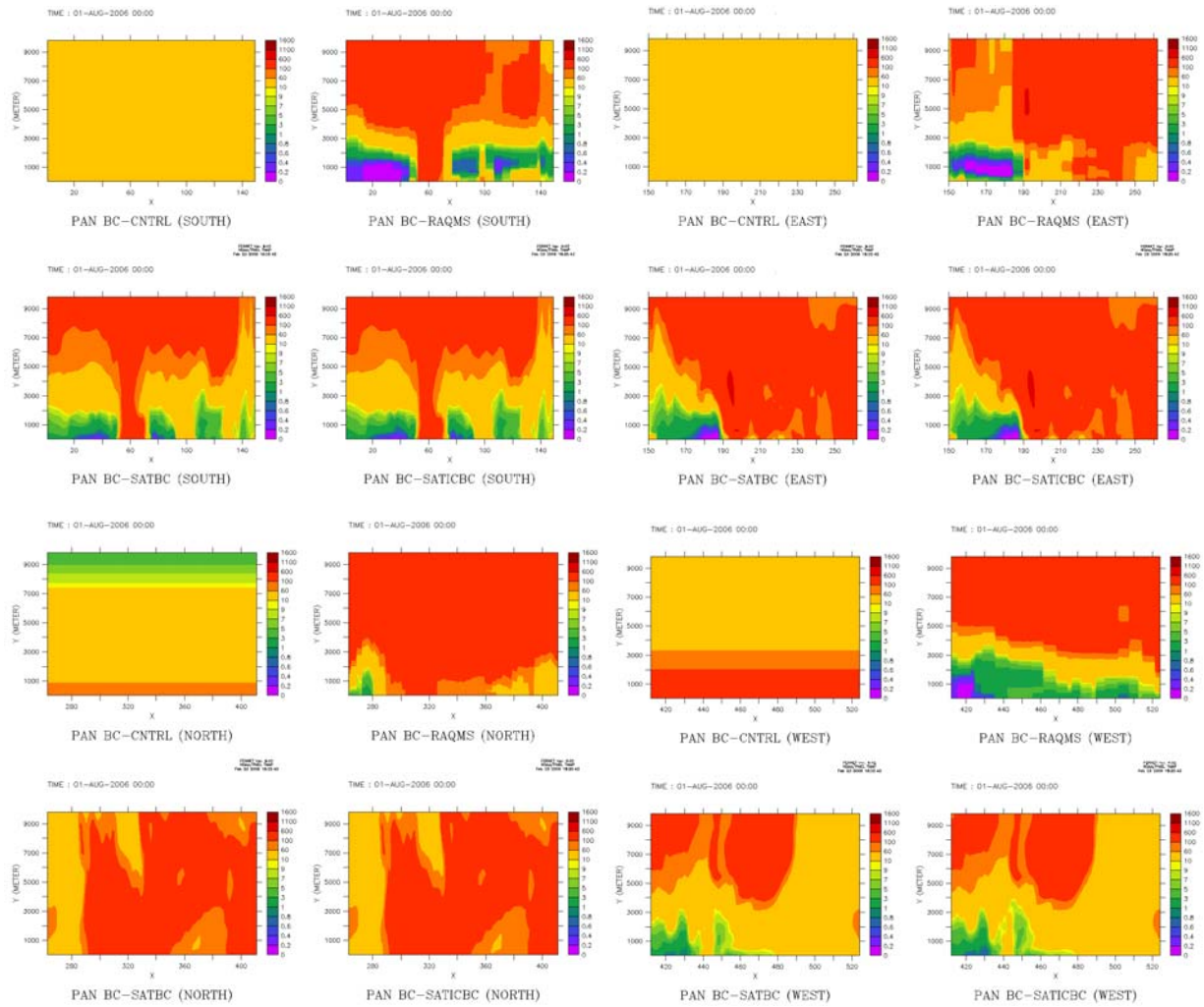


Figure 9– PAN (ppt) BC for south, east, north, and west boundaries. In each panel, BC for control (top left, standard CMAQ BC), RAQMS_BC (top right, BC from RAQMS global model), SAT_BC (lower left, BC from model) and SAT_ICBC (lower right) simulations for August 1, 2006 are presented. Note that BC for SAT_BC and SAT_ICBC are identical. They are both included for completeness.

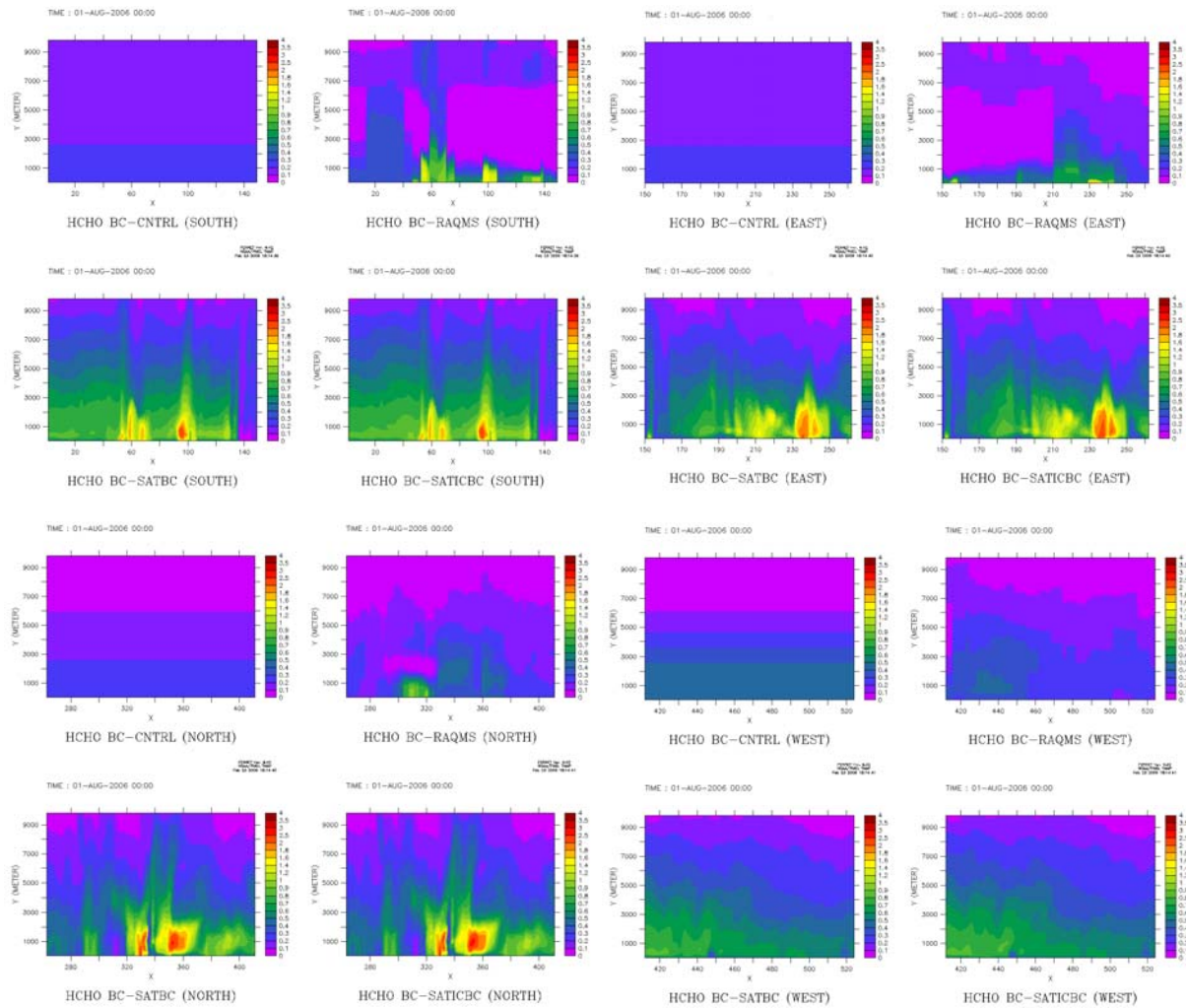


Figure 10- Formaldehyde (ppb) BC for south, east, north, and west boundaries. In each panel, BC for control (top left, standard CMAQ BC), RAQMS_BC (top right, BC from RAQMS global model), SAT_BC (lower left, BC from model) and SAT_ICBC (lower right) simulations for August 1, 2006 are presented. Note that BC for SAT_BC and SAT_ICBC are identical. They are both included for completeness.

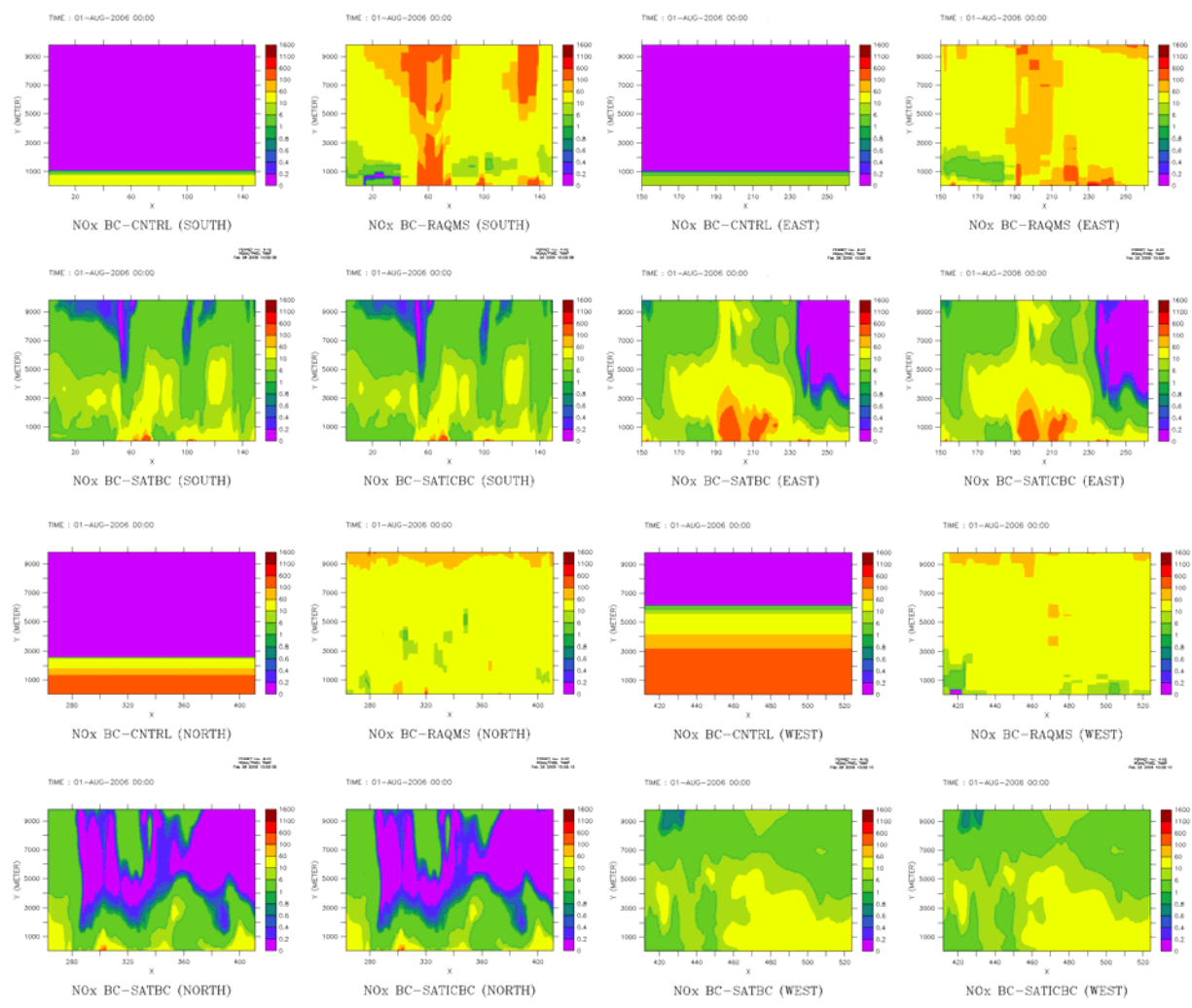


Figure 11– NO_x (ppt) BC for south, east, north, and west boundaries. In each panel, BC for control (top left, standard CMAQ BC), RAQMS_BC (top right, BC from RAQMS global model), SAT_BC (lower left, BC from model) and SAT_ICBC (lower right) simulations for August 1, 2006 are presented. Note that BC for SAT_BC and SAT_ICBC are identical. They are both included for completeness.

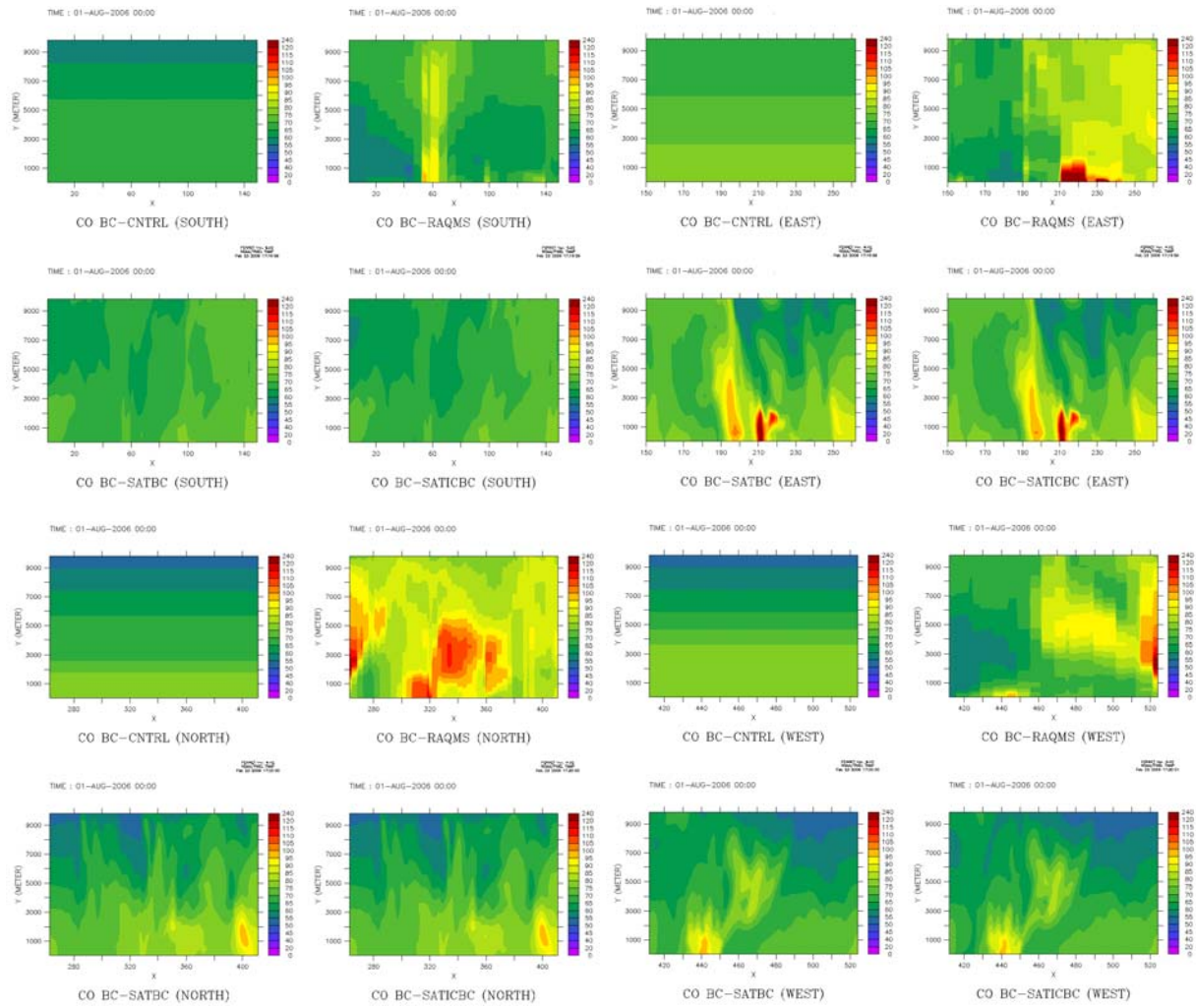


Figure 12– Carbon monoxide (ppb) BC for south, east, north and west boundaries. In each panel, BC for control (top left, standard CMAQ BC), RAQMS_BC (top right, BC from RAQMS global model), SAT_BC (lower left, BC from model) and SAT_ICBC (lower right) simulations for August 1, 2006 are presented. Note that BC for SAT_BC and SAT_ICBC are identical. They are both included for completeness.

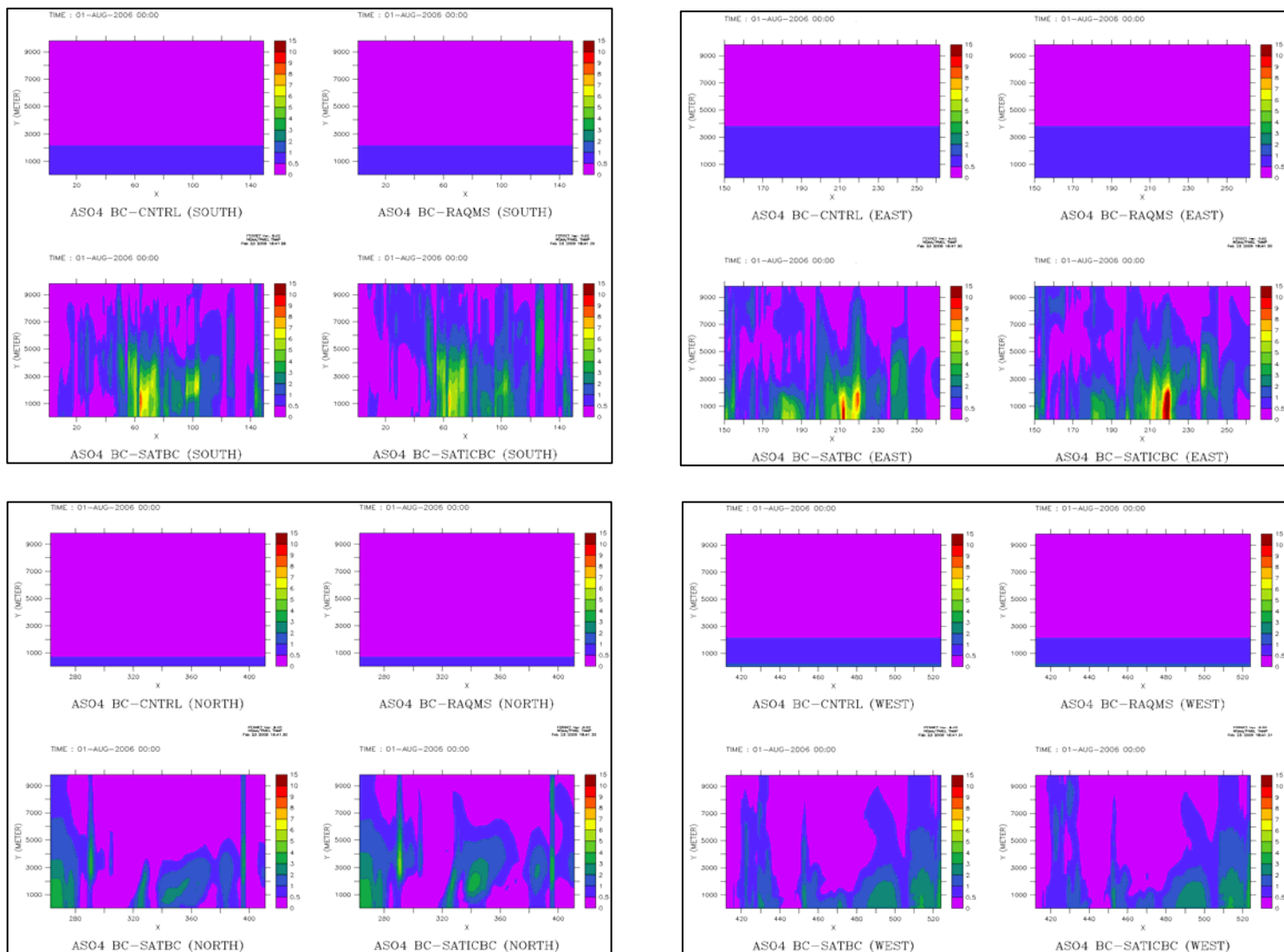


Figure 13– Sulfate aerosol ($\mu\text{g}/\text{m}^3$) BC for south, east, north and west boundaries. In each panel, BC for control (top left, standard CMAQ BC), RAQMS_BC (top right, BC from RAQMS global model), SAT_BC (lower left, BC from model) and SAT_ICBC (lower right) simulations for August 1, 2006 are presented. Note that BC for control and RAQMS_BC and for SAT_BC and SAT_ICBC are identical. They are included for completeness. CMAQ does not have the aerosol species from RAQMS mapped; therefore, the standard CMAQ concentrations are used.

F. Model performance evaluation

1. Methodology

We evaluated the performance of the model in the boundary layer using O_3 and $\text{PM}_{2.5}$ observations recorded at EPA's Air Quality System (AQS) sites. For performance above the boundary layer, we use ozonesonde observations recorded during the IONS06 field campaign.

The statistical measures include the Mean Bias (MB), Mean Error (ME), Mean Normalized Bias (MNB), Mean Normalized Error (MNE), Mean Fractional Bias (MFB), Mean Fractional Error (MFE) in hourly averaged concentrations predicted at these stations. Table 10 provides the mathematical formulation of these metrics. Since the normalized quantities can become large when observations are small, using a cut-off value is necessary while computing MNB and MNE statistics. The calculation excludes the prediction-observation pair whenever the observation is smaller than the cut-off value.

Table 10- Mathematical formulation of statistical metrics for model performance evaluation at surface.

Metrics	Formulation	Notes
Mean Bias (MB)	$\frac{1}{N} \sum_{i=1}^N (C_i^s - C_i^o) \times 100\%$	Computed for all valid observations.
Mean Error (ME)	$\frac{1}{N} \sum_{i=1}^N C_i^s - C_i^o \times 100\%$	Same as MB
Mean Normalized Bias (MNB)	$\frac{1}{N} \sum_{i=1}^N \frac{(C_i^s - C_i^o)}{C_i^o} \times 100\%$	Computed when observation is greater than the cut-off value, which is set at 60 ppb for Ozone and 1.0 ug/m ³ for PM _{2.5}
Mean Normalized Error (MNE)	$\frac{1}{N} \sum_{i=1}^N \frac{ C_i^s - C_i^o }{C_i^o} \times 100\%$	Same as MNB
Mean Fraction Bias (MFB)	$\frac{1}{N} \sum_{i=1}^N \frac{(C_i^s - C_i^o)}{C_i^s + C_i^o} \times 100\%$	Computed when observation is greater than the cut-off value, which is set at 60 ppb for Ozone and 1.0 ug/m ³ for PM _{2.5}
Mean Fraction Error (MFE)	$\frac{1}{N} \sum_{i=1}^N \frac{ C_i^s - C_i^o }{C_i^s + C_i^o} \times 100\%$	Same as MFB

2. CMAQ evaluation over total atmosphere column

The purpose of CMAQ evaluation is to know (1) how assimilation model performance correlates to satellite aerosol product, AOT, (2) how much bias in the assimilation data from MODIS data in an assumption that data from satellite are correct, and (3) variance of assimilation data over CONUS. Correlation is increasing and mean normalized bias (MNB) and variance is reducing. Figure 14 shows the model performance compared to MODIS satellite data.

Many pixels of baseline model (CNTRL) are under-predicted compared to satellite data, especially when MODIS AOT is less than 0.6 and the results show baseline model performance does not capture aerosol properly (Figure 15-(a)). Assimilation model data catch satellite data well and scattering is following to 1:1 line. If AOT is less than 0.6, low model values of AOT at baseline become high values at assimilation model. (Figure 15-(b)).

- Correlation

$$r = \frac{\frac{1}{N-1} \sum (C_M - \bar{C}_M)(C_o - \bar{C}_o)}{\sqrt{\frac{1}{N-1} \sum (C_M - \bar{C}_M)^2} \sqrt{\frac{1}{N-1} \sum (C_o - \bar{C}_o)^2}}$$

- Mean Normalized Bias

$$MNB = \frac{1}{N} \sum \left(\frac{C_M - C_o}{C_o} \right)$$

- Variance

$$Variance = \frac{\sum (C_M - C_o)^2}{N-1}$$

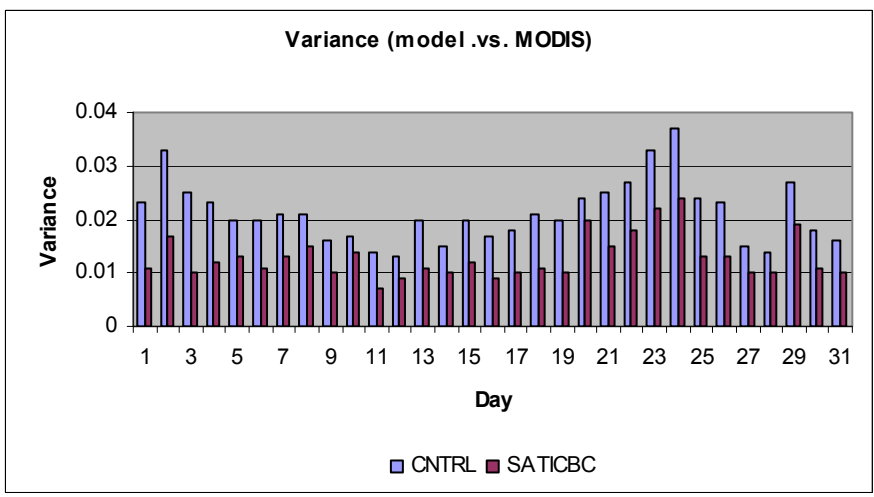
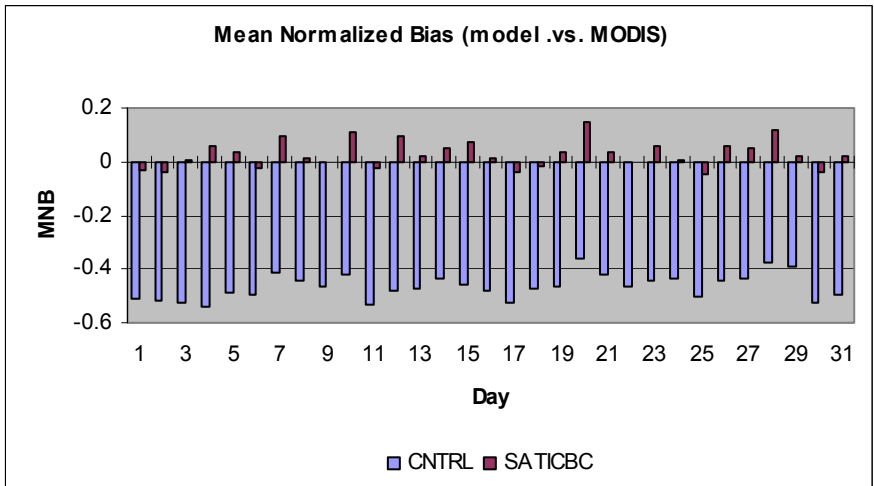
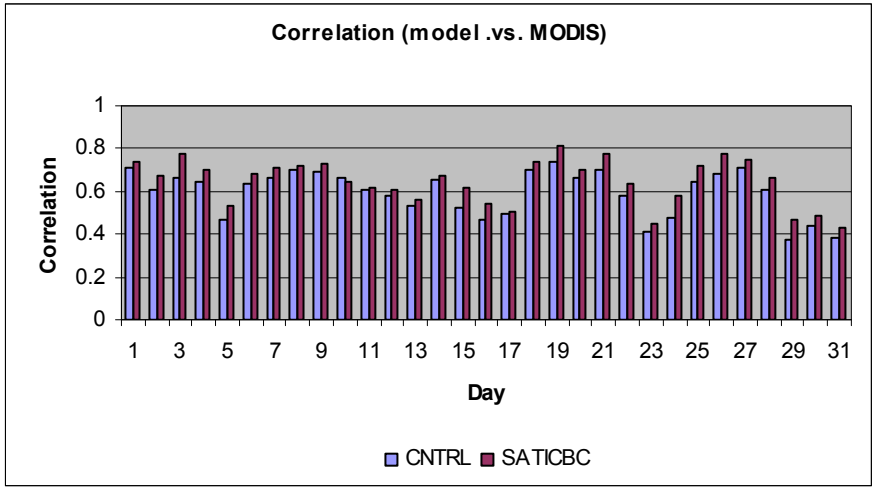


Figure 14- Statistics of CNTRL model and SATICBC.

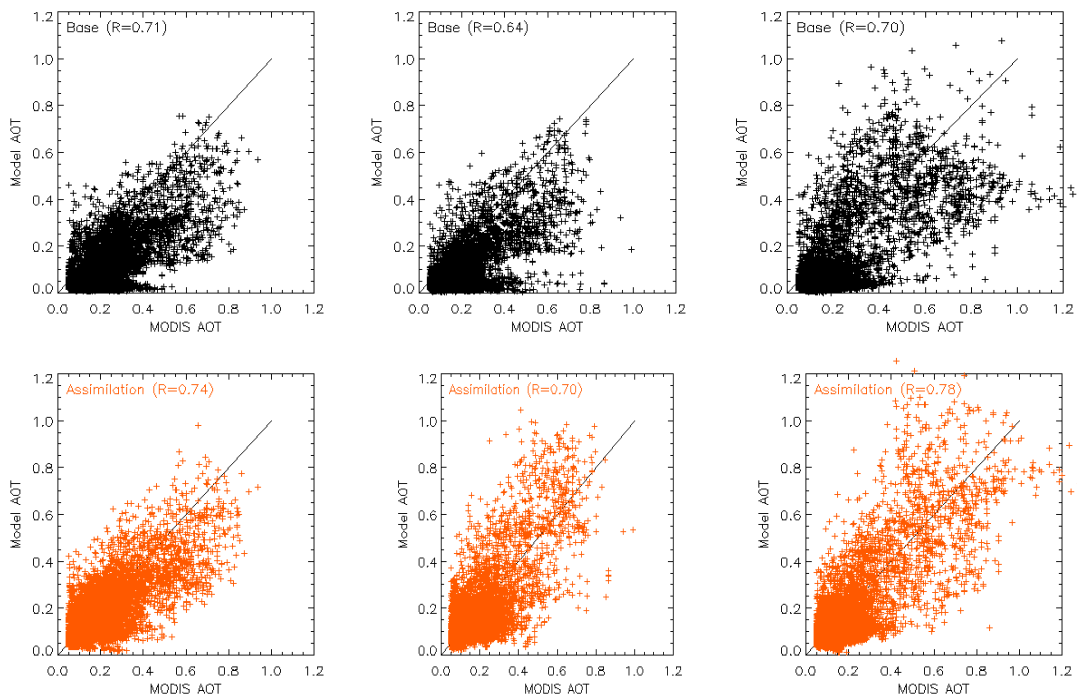


Figure 15- Scatter plot for MODIS AOT versus modeled AOT (first row (13-(a)) is for baseline model and second row (13-(b)) is for assimilation model.)

3. Surface evaluation

Spatial evaluations of west area, central area, and east area show improvement of model performance in comparison to mass concentration of surface observations. Some states, which represent those three areas, show better correlation and less MNB and variance (Figure 16). The states for evaluation can be represented as west (California (CA) and Idaho (ID)), mid-east ((or centre – Texas (TX)) and south-east ((Mississippi (MS), North Carolina (NC), Alabama (AL), Georgia (GA), Tennessee (TN)).

Baseline model performance is not poor in east areas but is poor in central and west areas. The model under predicts PM25 at most regions in the west U.S., but the assimilation model performance of aerosol is improved even in west areas.

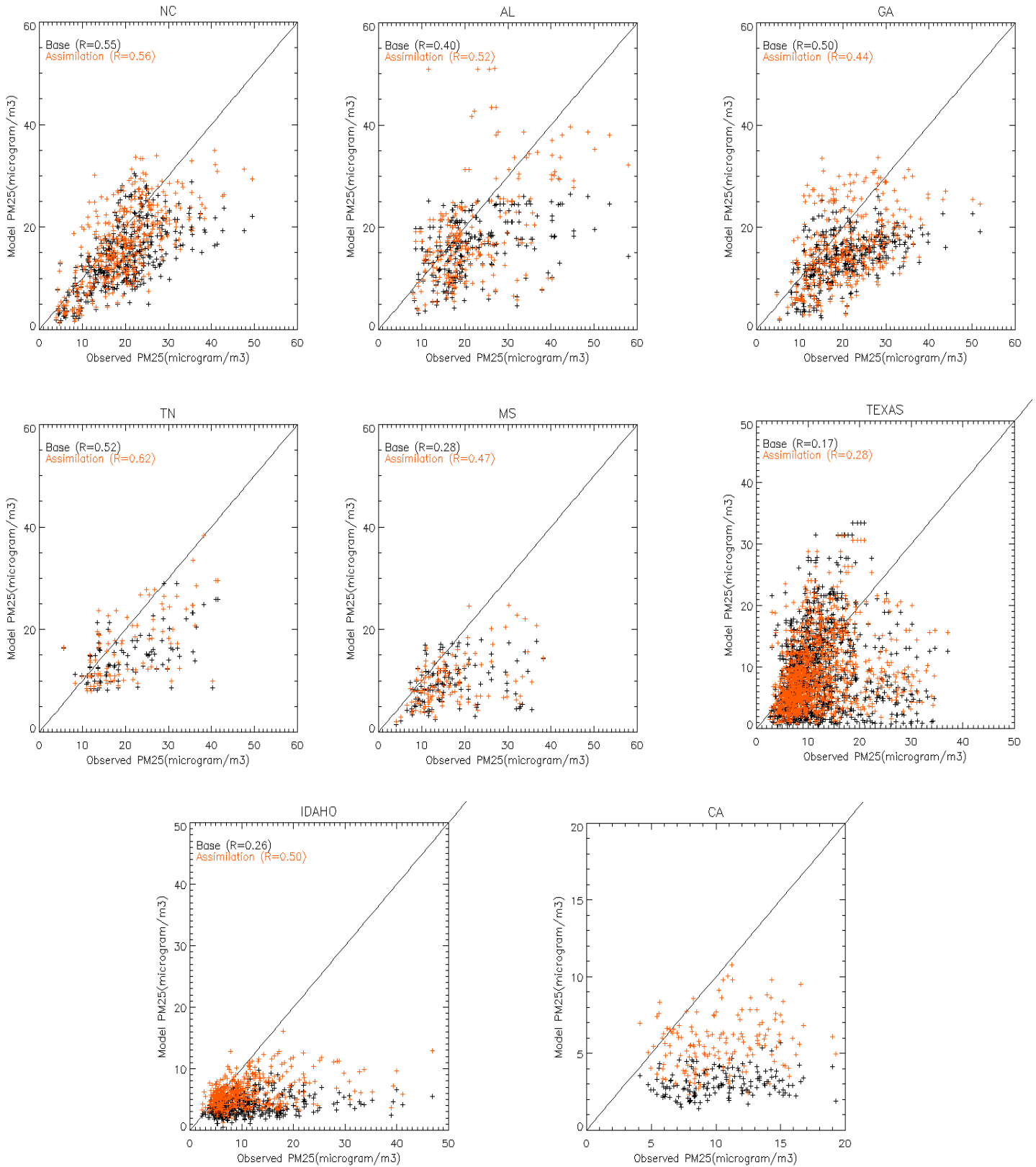


Figure 16- Comparison of observed PM25 at ground level and model-predicted PM25 at surface of daily PM25 values during August 2006.

Monthly mean statistics comparing model-simulated surface PM_{2.5} to the surface observations also show improvement. Figure 17, Figure 18, and Figure 19 show the statistics for different sub-regions indicated in Figure 2. As indicated in the charts, the model under-predicts PM_{2.5} in all regions. MODIS aerosol products improve the outcome; however, the improvement is not uniform in all regions. Using MODIS observations in specifying both the lateral boundary conditions and the initial condition (for each 24 hr run segment) has the greatest impact across all regions.

The overall evaluation of the results indicates that the model performance with respect to the prediction of PM_{2.5} total mass is greatly improved. Since the scaling assumes that the model partitioning and distribution of PM_{2.5} species is reasonable and the error is due to the magnitude of emissions/transformation, in cases where the partitioning was inaccurate, the model exacerbated the inaccuracies. Our future research in this area will try to utilize the data from surface monitors to complement satellite observations and attempt to correct the PM_{2.5} partitioning as well as scaling.

The top panel in Figure 17 shows the mean observed mass concentration of PM_{2.5} for different regions versus model predictions from CNTRL, RAQMS, SATBC, and SATICBC simulations. SATICBC simulation shows a marked improvement over CNTRL in predicting PM_{2.5} in all regions and particularly in the Mid-Atlantic/Northeast region where the bias is practically negligible. Figure 17 shows the overall mean bias and error. The statistics demonstrate that while the use of satellite observations for BC marginally improves model performance, readjusting PM_{2.5} every 24 hours can significantly enhance model predictions of PM_{2.5}. This is an expected result because correcting BC greatly affects the regions closer to the lateral boundaries of the domain, but initializing the model simulation with a satellite-derived field corrects the total mass in the entire domain. Figure 18 and Figure 19 present the improvements made by removing the smaller concentrations where monthly mean normalized and fractional bias and error exist. For example, the overall MFB shows a 30 % reduction.

Figure 20 and Figure 21 show the daily averaged difference in PM_{2.5} mass concentration between RAQMS, SATBC and SATICBC simulations and the CNTRL simulation for August 20 and 24, 2006. A more detailed analysis of the results shows that episodically the satellite derived BC also significantly impact PM_{2.5} over a large region and is able to explain the impact of large-scale transport. Figure 22 shows one such event where there is a large influx of PM_{2.5} from the southeastern boundary impacting the Gulf of Mexico, Louisiana, Texas, Oklahoma, Arkansas, and extending into Kansas and Missouri. Events showing the impact of PM_{2.5} transport are common. However, since in such events the transport is the dominant factor, the accuracy of model predictions of PM_{2.5} is dependent on the ability of the meteorological model in explaining the flow field.

SATICBC simulation shows the largest deviation from the CNTRL simulation in the eastern part of the domain particularly on August 24, 2006. RAQMS simulation also shows the increase in the eastern part of the domain for this day, but the magnitude of the increase is not adequate to explain the model under-prediction.

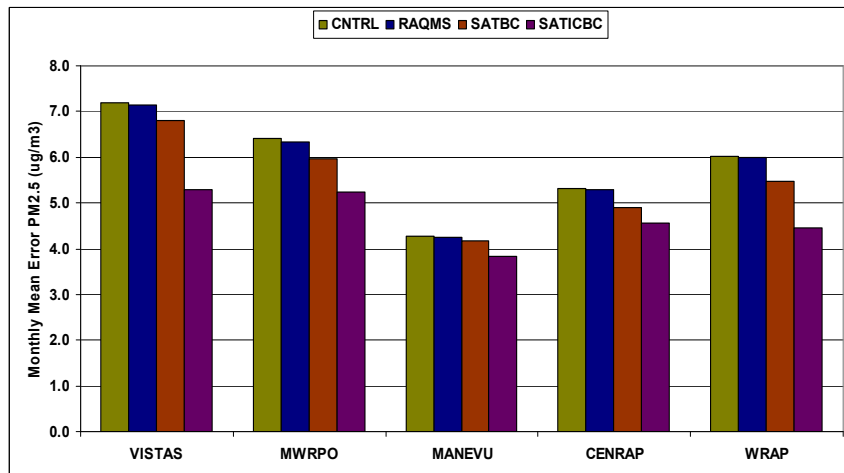
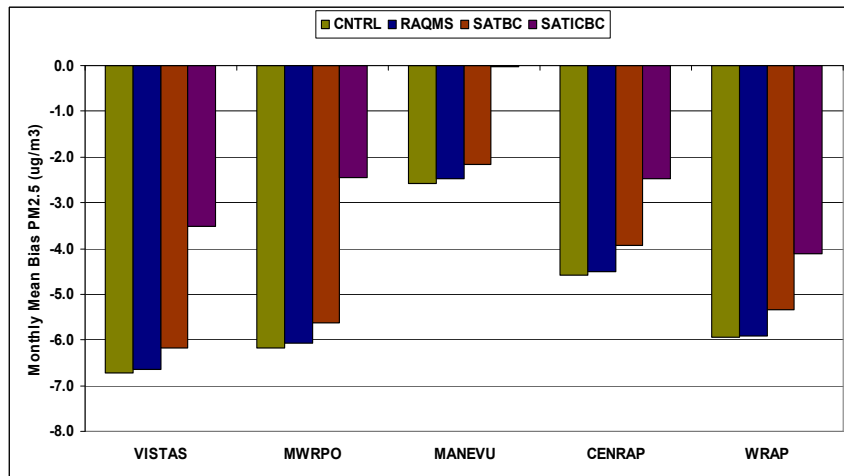
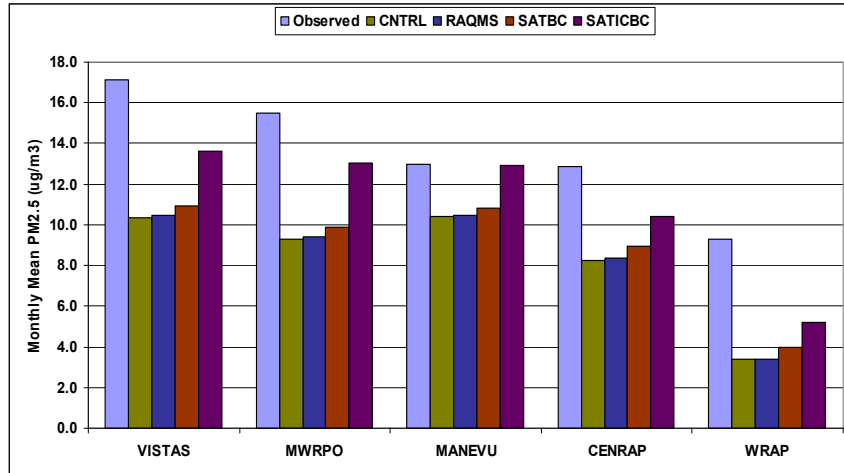


Figure 17 – Charts showing the monthly mean, mean bias and mean error for model simulated PM_{2.5} for different regions (as indicated in Figure 2). Midwest and Mid-Atlantic/Northeast regions show the greatest improvement in performance.

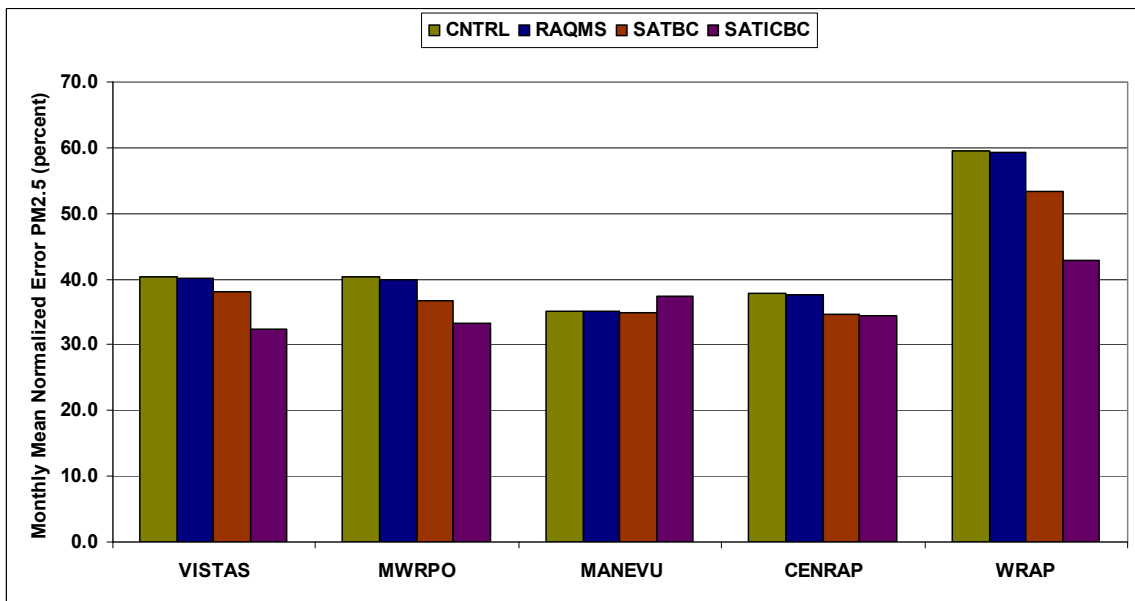
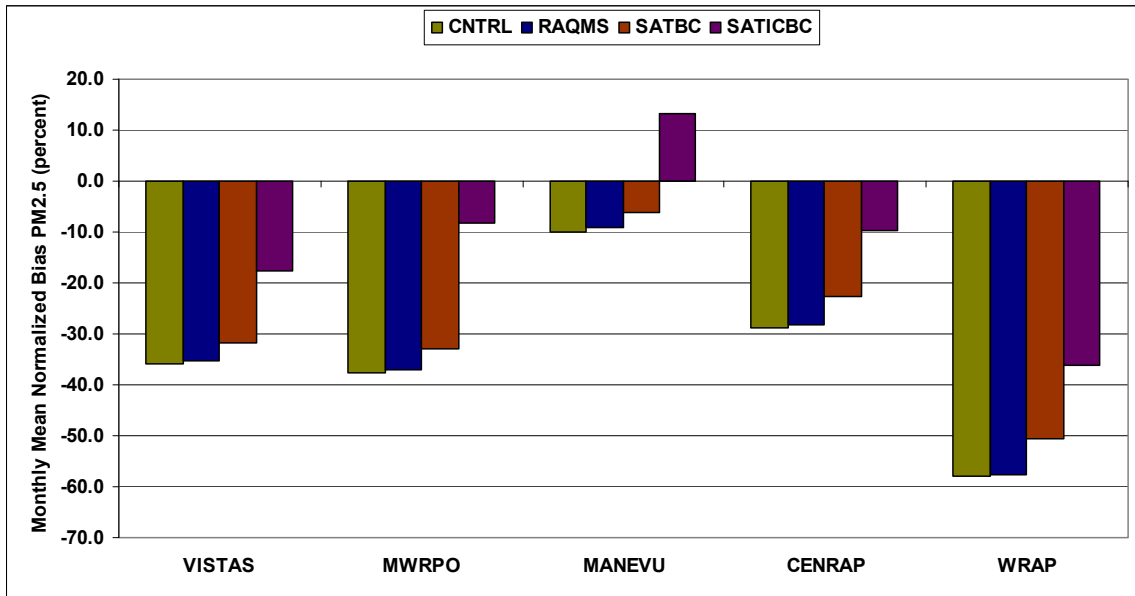


Figure 18 – Monthly mean normalized bias and error for model simulated PM2.5 for the month of August 2006 for different sub-regions (as indicated in Figure 2).

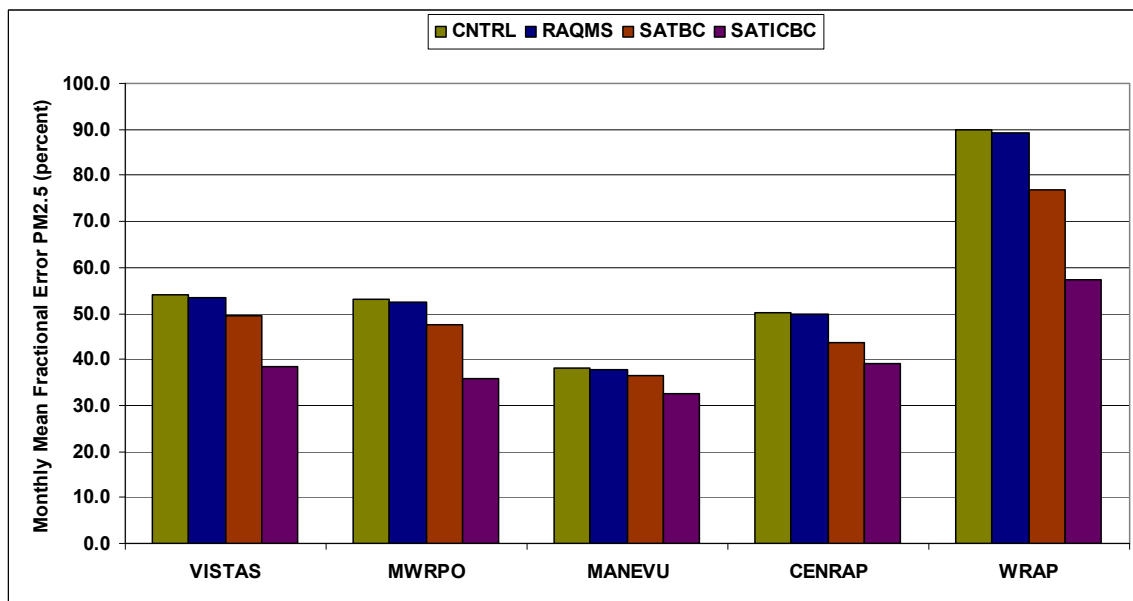
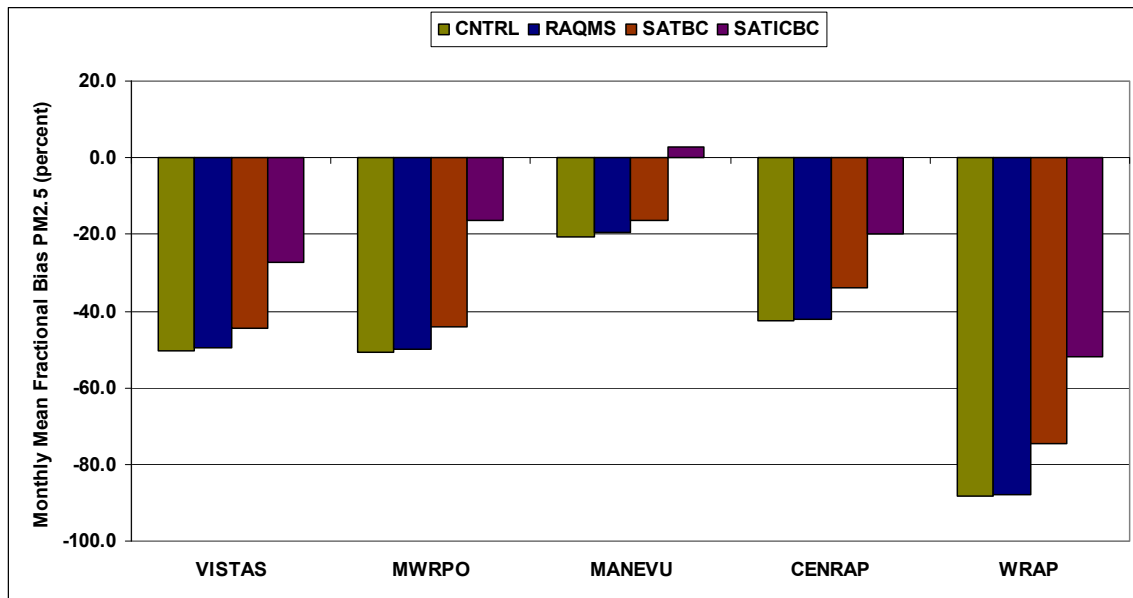


Figure 19 – Monthly mean fractional bias and error for model simulated PM2.5 for August 2006 for different sub-regions (as indicated in Figure 2).

1. Result of aerosol simulation

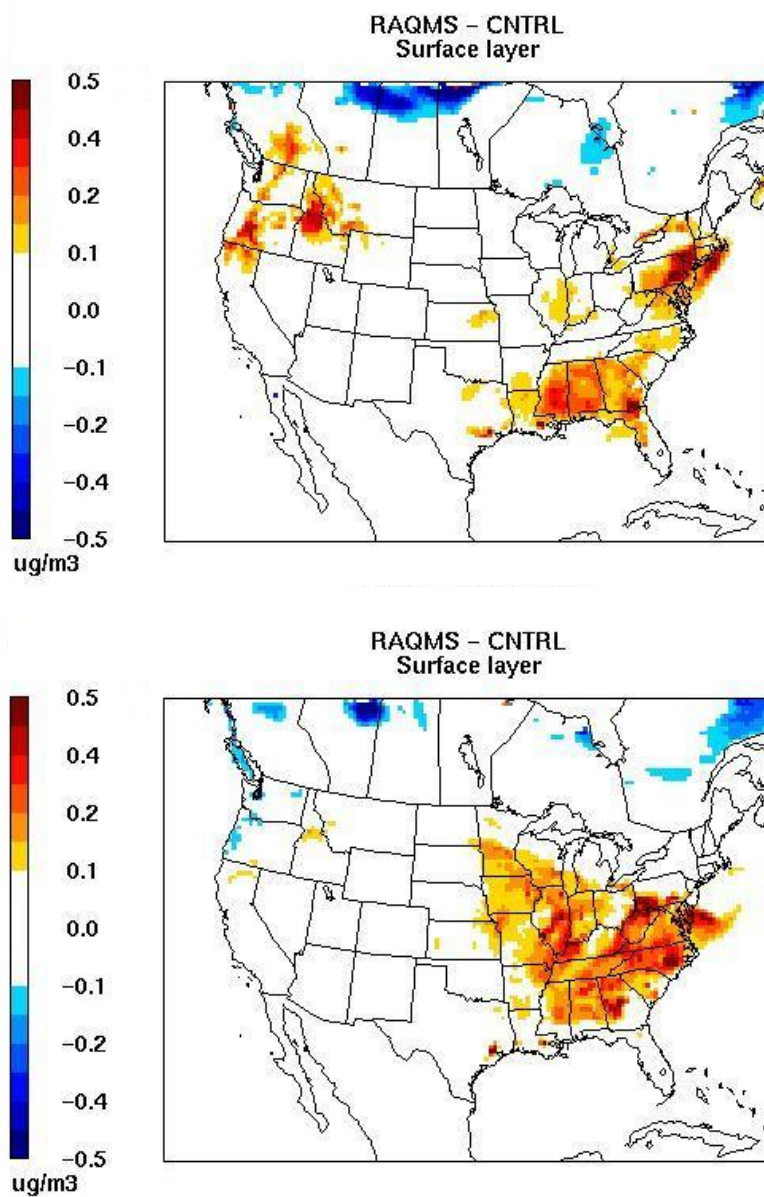


Figure 20- Daily average difference in surface layer PM2.5 concentration (RAQMS minus CNTRL) for August 20 (top) and August 24, 2006 (bottom).

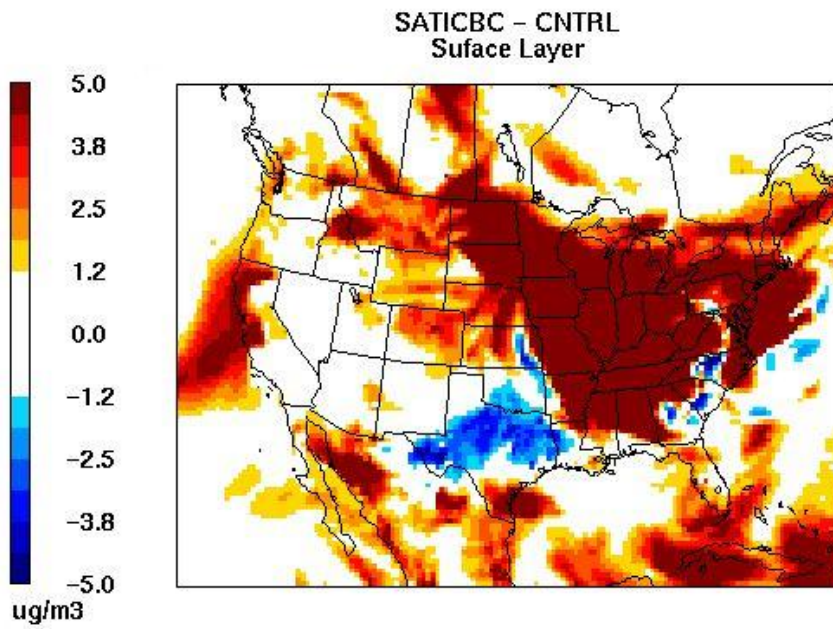
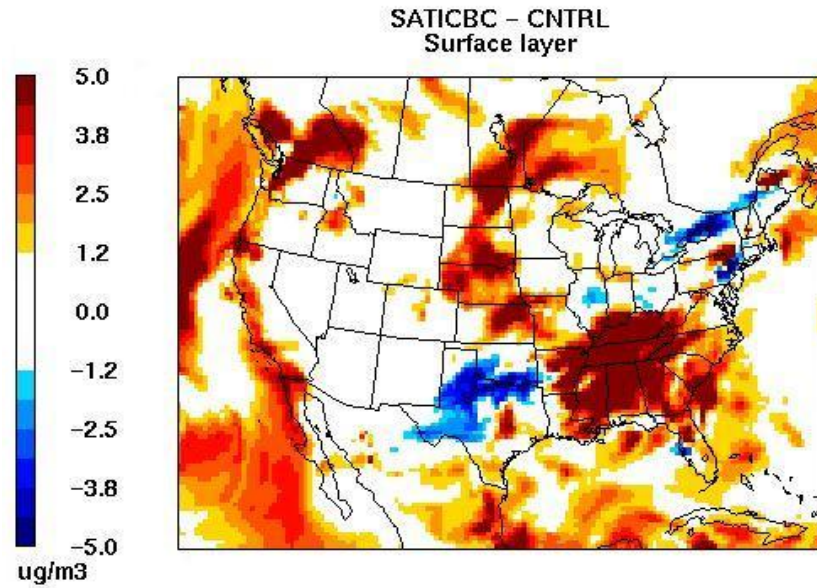


Figure 21 - Daily average difference in surface layer PM_{2.5} concentration (RAQMS minus CNTRL) for August 24, 2006 (bottom).

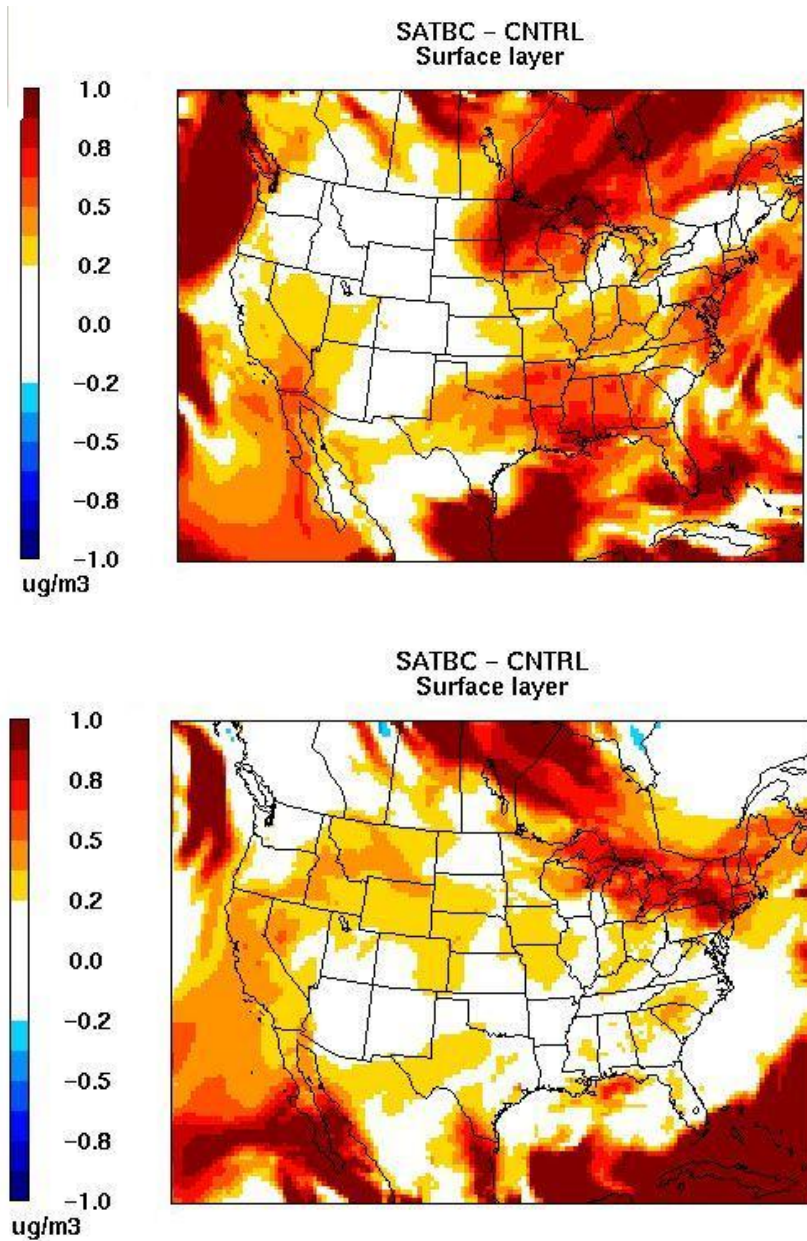


Figure 22 - Daily average difference in surface layer PM2.5 concentration (SATBC minus CNTRL) for August 20 (top) and August 24, 2006 (bottom).

2. Result of ozone simulation

EPA monitoring stations evaluated the performance of the model. The statistical measures include the Mean Bias (MB), Mean Error (ME), Mean Normalized Bias (MNB), Mean Normalized Error (MNE), Mean Fractional Bias (MFB), and Mean Fractional Error (MFE) in hourly averaged concentrations predicted at these stations. Table 10 provides the mathematical formulation of the metrics. Since the normalized quantities can become large when observations are small, a cut-off value of 60, 10, and 120 ppb for O₃, SO₂, and CO, respectively, assist in computing MNB and MNE statistics. Thus, whenever the observation is smaller than the cut-off value, the calculation excludes the prediction-observation pair. The study presents the hourly-normalized bias and error metrics as daily averages over all monitoring stations. Thus, whenever the observation is smaller than the cut-off value, the calculation excludes the prediction-observation pair.

The CNTRL simulation will serve as the comparison reference point to other simulations. Table 11 presents the statistics from CNTRL run for the five sub-regions shown in Figure 2. Bias for all sub-regions is about 6 ppb with the normalized bias being -7 % for the Midwest region. The systematic over-prediction of ozone at night in CMAQ causes the positive bias. CMAQ over-predicts ozone at night and under-predicts it during the daytime peaks. Since MNB does not include the lower values at night, it shows an under-prediction of 7-12 % for different sub-regions. The under-prediction is the lowest in the Midwest region at 7 %, followed by 9 % in the Mid-Atlantic/Northeast region, 10 % in the Central region, 11 % in the Southeast region, and 12 % in the Western region.

Table 11 - Performance statistics for CNTRL simulation (August 1-31, 2006 at 36-km grid resolution)

			CENRAP	MANEVU	MWRPO	VISTAS	WRAP
Ozone	Mean OBS	ppm	0.033	0.033	0.029	0.034	0.034
Ozone	Mean PRD	ppm	0.039	0.039	0.037	0.039	0.039
Ozone	Bias	ppm	0.006	0.006	0.007	0.006	0.006
Ozone	Gross Error	ppm	0.012	0.012	0.013	0.012	0.012
Ozone	Normalized Bias	percent	-10.237	-9.391	-6.670	-11.063	-11.736
Ozone	Normalized Error	percent	18.813	17.566	19.235	18.508	18.983
Ozone	Fractional Bias	percent	23.995	23.812	27.019	22.513	22.680
Ozone	Fractional Error	percent	41.828	44.028	49.349	43.363	43.196
Carbon monoxide	Mean OBS	ppm	0.427	0.402	0.483	0.371	0.448
Carbon monoxide	Mean PRD	ppm	0.245	0.237	0.205	0.266	0.246
Carbon monoxide	Bias	ppm	-0.182	-0.165	-0.277	-0.105	-0.202
Carbon monoxide	Gross Error	ppm	0.241	0.234	0.345	0.212	0.270
Carbon monoxide	Normalized Bias	percent	-33.972	-33.976	-42.872	-23.469	-33.961
Carbon monoxide	Normalized Error	percent	50.324	50.808	67.090	50.824	52.118
Carbon monoxide	Fractional Bias	percent	-44.007	-38.339	-70.929	-29.888	-45.017
Carbon monoxide	Fractional Error	percent	66.461	68.789	87.253	61.826	69.104
Sulfur dioxide	Mean OBS	ppm	0.004	0.004	0.003	0.003	0.004
Sulfur dioxide	Mean PRD	ppm	0.004	0.005	0.004	0.004	0.004
Sulfur dioxide	Bias	ppm	0.000	0.001	0.001	0.000	0.000
Sulfur dioxide	Gross Error	ppm	0.004	0.004	0.003	0.003	0.004
Sulfur dioxide	Normalized Bias	percent	-57.305	-55.845	-60.830	-54.028	-60.745
Sulfur dioxide	Normalized Error	percent	68.321	63.033	67.123	61.995	67.389
Sulfur dioxide	Fractional Bias	percent	17.045	17.426	34.238	1.216	5.386
Sulfur dioxide	Fractional Error	percent	85.776	84.547	79.457	81.569	80.420

Comparing the other simulations to the control offers mixed result. Some metrics show improvements, while the others indicate deterioration. However, the overall picture is consistent and indicates an overall increase in ozone concentration in RAQMS, SATBC and SATICBC simulations. That is, the nighttime over-prediction is exacerbated, but the daytime under-prediction is improved. Figure 23 shows the mean observed concentration for each sub-region (and the overall) along with model predictions for August 2006. RAQMS over-predicts ozone in all regions while SATBC and SATICBC exhibit a better agreement with the average observations for MANEVU and CENRAP regions. The average concentrations represent daytime, as well as nighttime observation/prediction pairs. As mentioned before, much of the over-prediction is due to the nighttime over-prediction. Figure 24 illustrates the Mean Normalized Bias (MNB) for different simulations. Because data pairs where observed ozone is less than 60 ppb are not included in the MNB calculation, this metric is an indicator of model performance with respect to daytime ozone prediction (or peak ozone prediction). Therefore, by eliminating the low nighttime values, Figure 24 shows that the model is under-predicting peak ozone. RAQMS simulation, which has the highest Mean Bias (MB), as illustrated in Figure 25 has the best overall performance during the day as evident from MNB (with the best performance in the Midwest region). SATBC and SATICBC simulations overall perform better than the control simulation but cannot outperform RAQMS. Judging from these statistics it seems that the satellite-derived boundary condition for the western boundary is much higher than what the surface observations indicate. Then, the predominant west-east flow is transporting the higher ozone to the east and its impact diminishes as the flow reaches the eastern part of the domain. In fact, both SATBC and SATICBC simulations perform poor in the west (WRAP) and outperform RAQMS in the southeast region (VISTAS) with respect to daytime ozone predictions. The BC in the southeastern part of the domain predominantly affects this region, and the daytime satellite profile explains the impact of transboundary flow to this region.

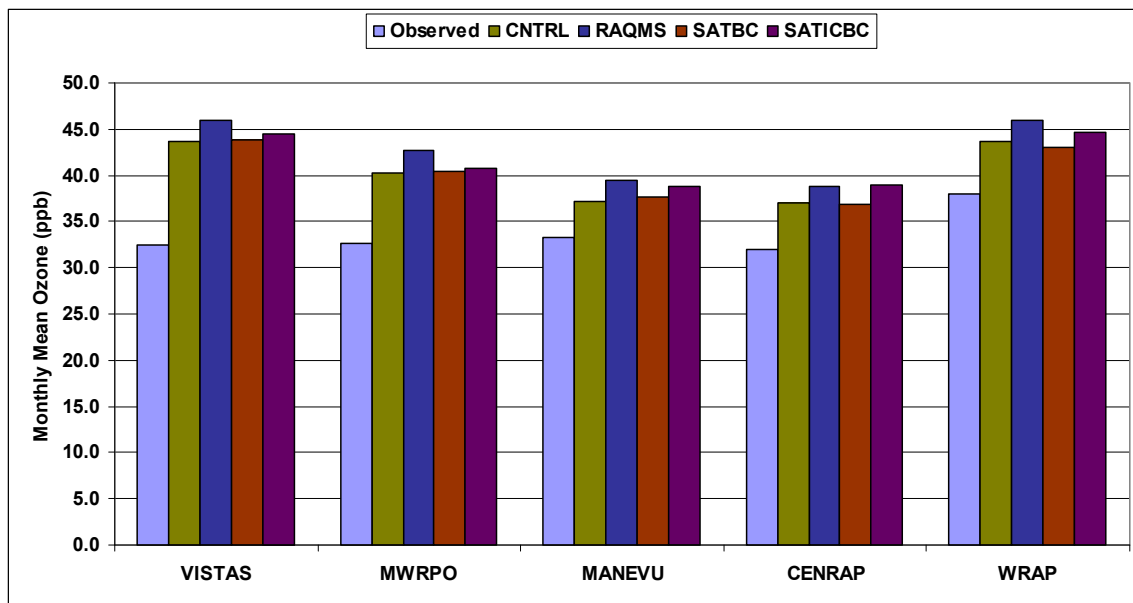


Figure 23 – Monthly mean ozone concentration from surface observations and model simulated values for each sub-region during the month of August 2006.

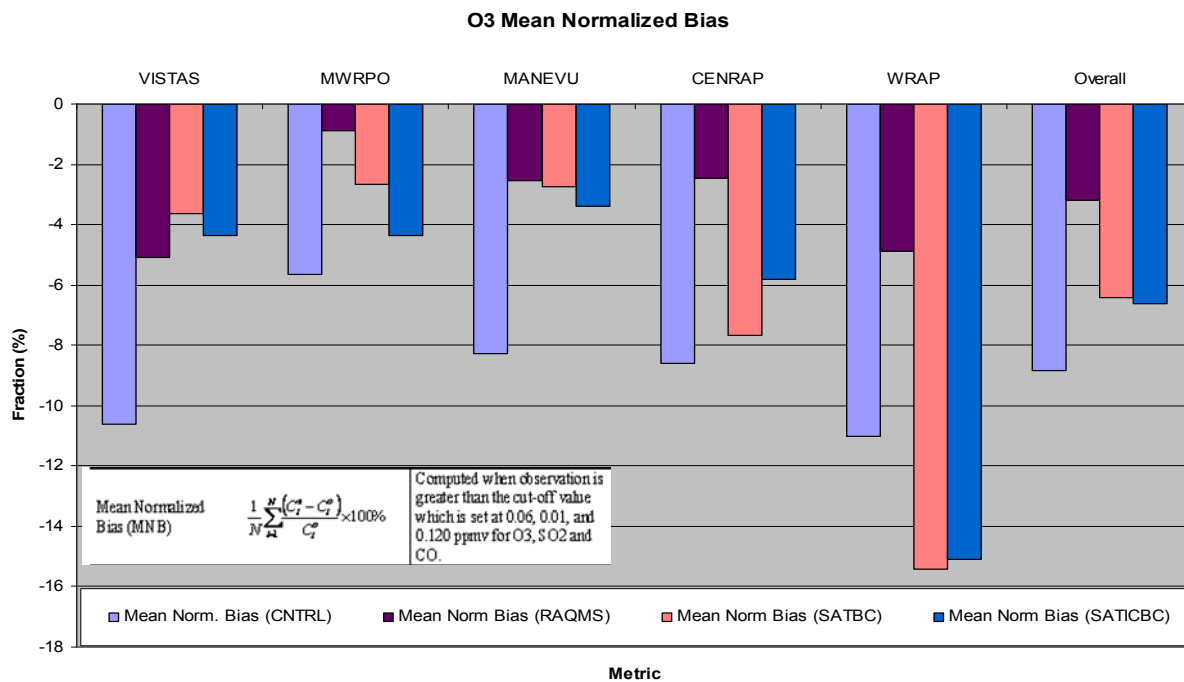


Figure 24 - Monthly mean normalized bias from each simulation for each sub-region during the month of August 2006.

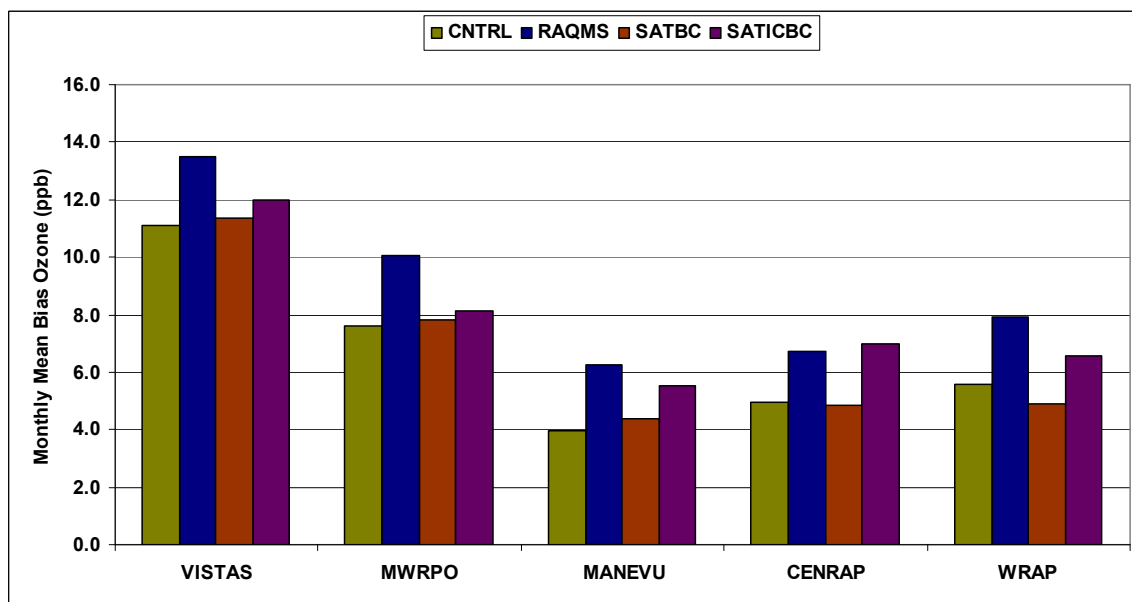


Figure 25 - Monthly mean bias for simulated ozone concentrations as compared to EPA surface observations for each sub-region.

Figure 26 is a snapshot of the difference in ozone concentration in the boundary layer (1 km altitude) between SATBC and the CNTRL simulations for August 16, 2006. The plot clearly shows the role of transport in advecting ozone from the lateral boundaries into the interior of the domain. It also shows higher ozone concentrations entering the interior of the domain from the northwestern boundary while the easterlies more affect the Southeast. This could partly explain the statistics discussed previously. A closer look at the role of transport and the impact of the boundary conditions reveals that the southeast region and the GoM area is more impacted by these easterlies that at times carry the remnants of the northeast pollution through re-circulation.

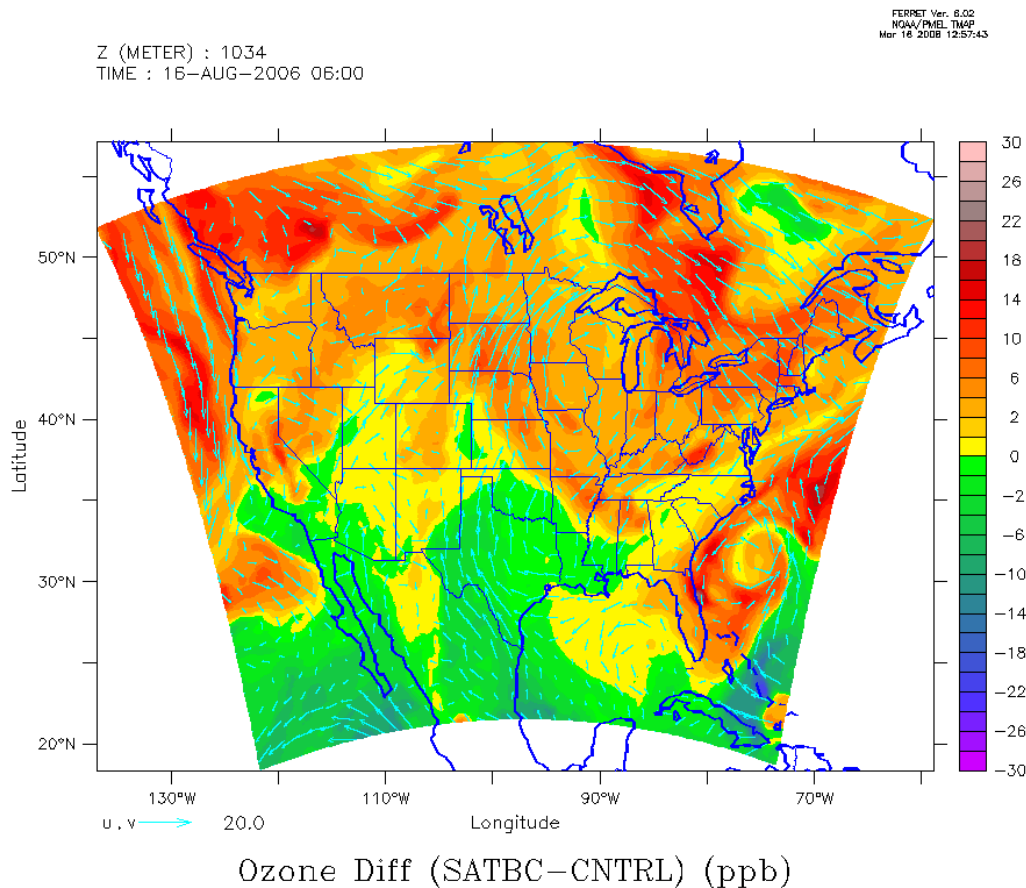


Figure 26 – Difference in ozone concentrations between SAT_BC and CNTRL simulations in the boundary layer for August 16, 2006. The plot clearly shows the role of transport in advecting ozone from the lateral boundaries

a. Evaluation of ozone simulation against ozonesonde measurements

We used 341 ozonesonde profiles for August 2006 from 18 stations that participated in the IONS06 campaign. One of these 18 stations is the NOAA research vessel Ron Brown located in The Gulf of Mexico for IONS06 and referred to as "Ron Brown station".

For each day during August 2006, the study compares ozonesonde measurements between 1500~2300 UTC with ozone mixing ratios at 1900 UTC simulated by four CMAQ runs. The base run significantly underestimates ozone concentrations in the upper troposphere, while ozone values simulated from RAQMS_bc, sat_bc, and sat_icbc look much closer to those measured by ozonesondes (Figure 27). The bottom left panel of Figure 27 illustrates the further improvement that results in the interior region by applying satellite data as IC (sat_icbc run). For example, at Huntsville, AL, ozone variations simulated from sat_icbc run show the best agreement with ozonesonde measurements (Figure 28).

Corresponding vertical distribution of ozone mixing ratios from four CMAQ simulations (cntrl, RAQMS_bc, sat_bc, sat_icbc) are compared with these ozonesonde profiles by calculating the relative differences $((\text{model-sonde}) \times 100/\text{sonde} \%)$ of each model-sonde pair, the mean of these relative differences (Mean Normalized Bias), and estimated error in calculating the mean values (Figure 29). The sat_bc performs the best between surface and 900 mb. The sat_icbc performs the best within 870 mb ~ 815 mb and 340mb ~ 240 mb. Between 800 mb ~ 375 mb, RAQMS_bc is the best. OMI ozone profiles are also evaluated with this ozonesonde data and show good agreement $(-10\% < \text{Mean Normalized Bias} < 10\%)$ except in the boundary layer region (surface to ~1.5km above ground) where the sample sizes (number of coincidence pairs between OMI and Ozonesonde profiles) are too small for a significant comparison (Table 12).

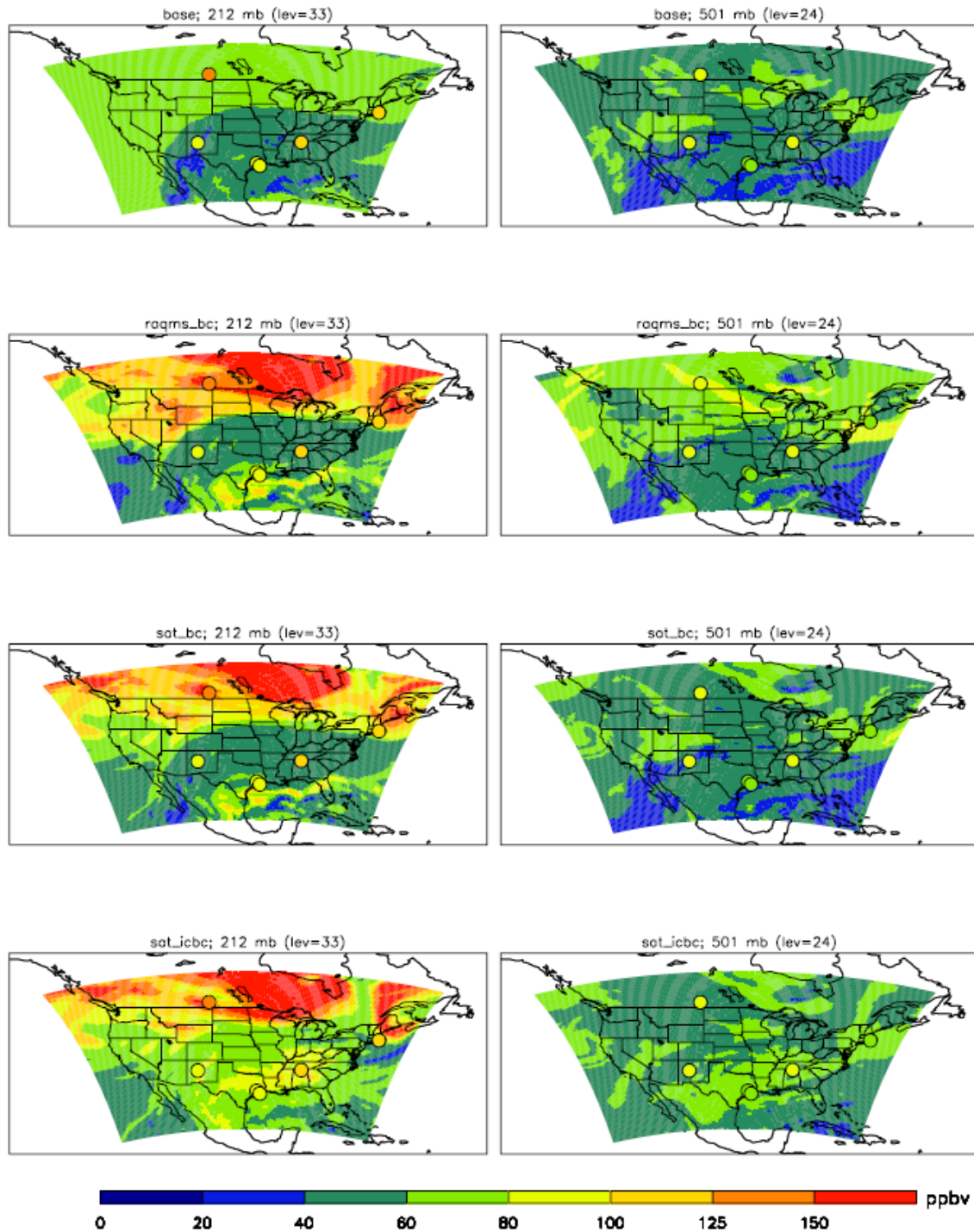


Figure 27- O₃ (ppbv) at 1900 UTC, August 21, 2006 simulated by 4 CMAQ runs; over plotted with 6 ozonesondes launched between 1500~2300 UTC. Left panels represent CMAQ level 33 (212 hPa). Right panels represent level 24 (501 hPa).

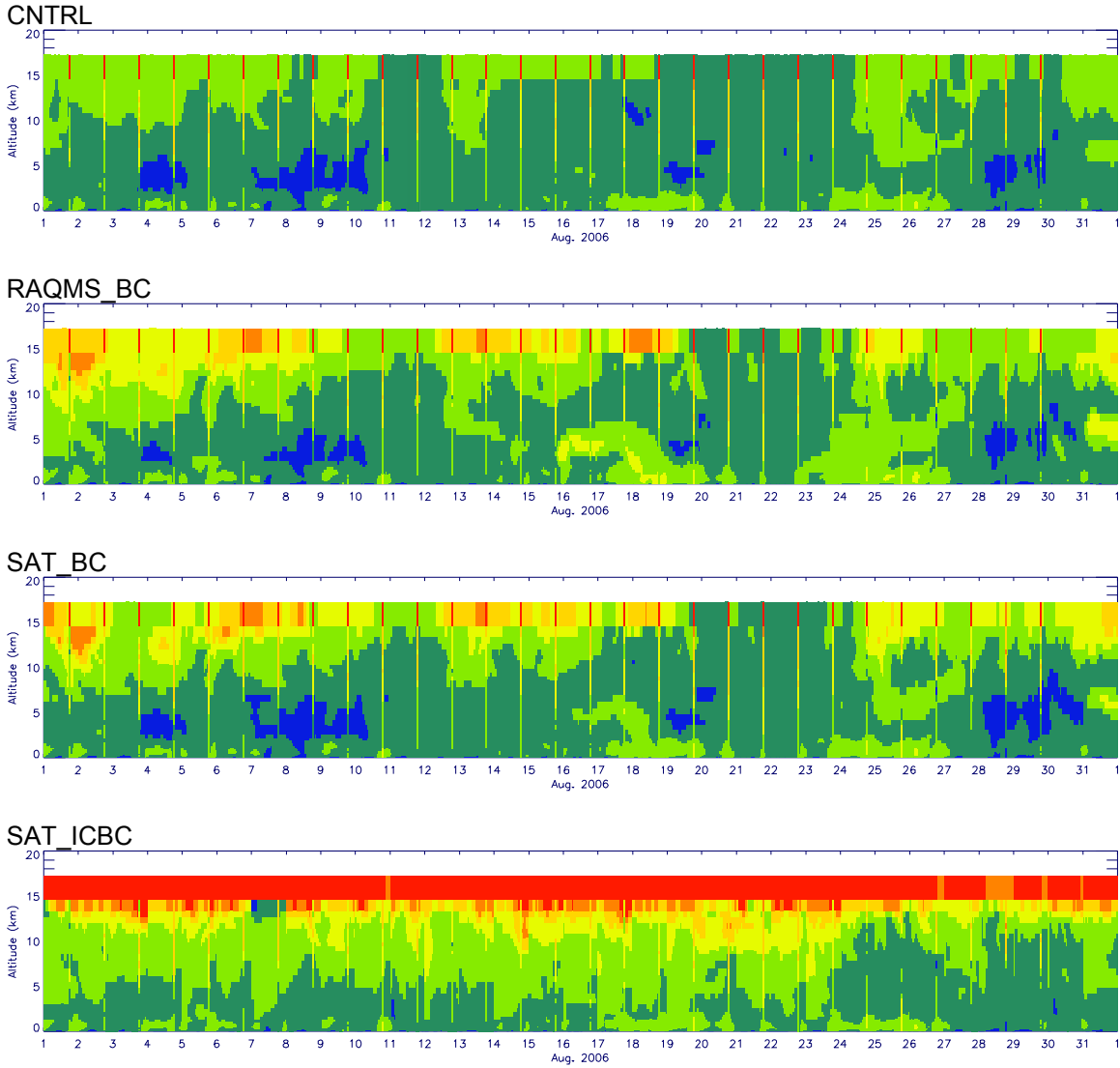
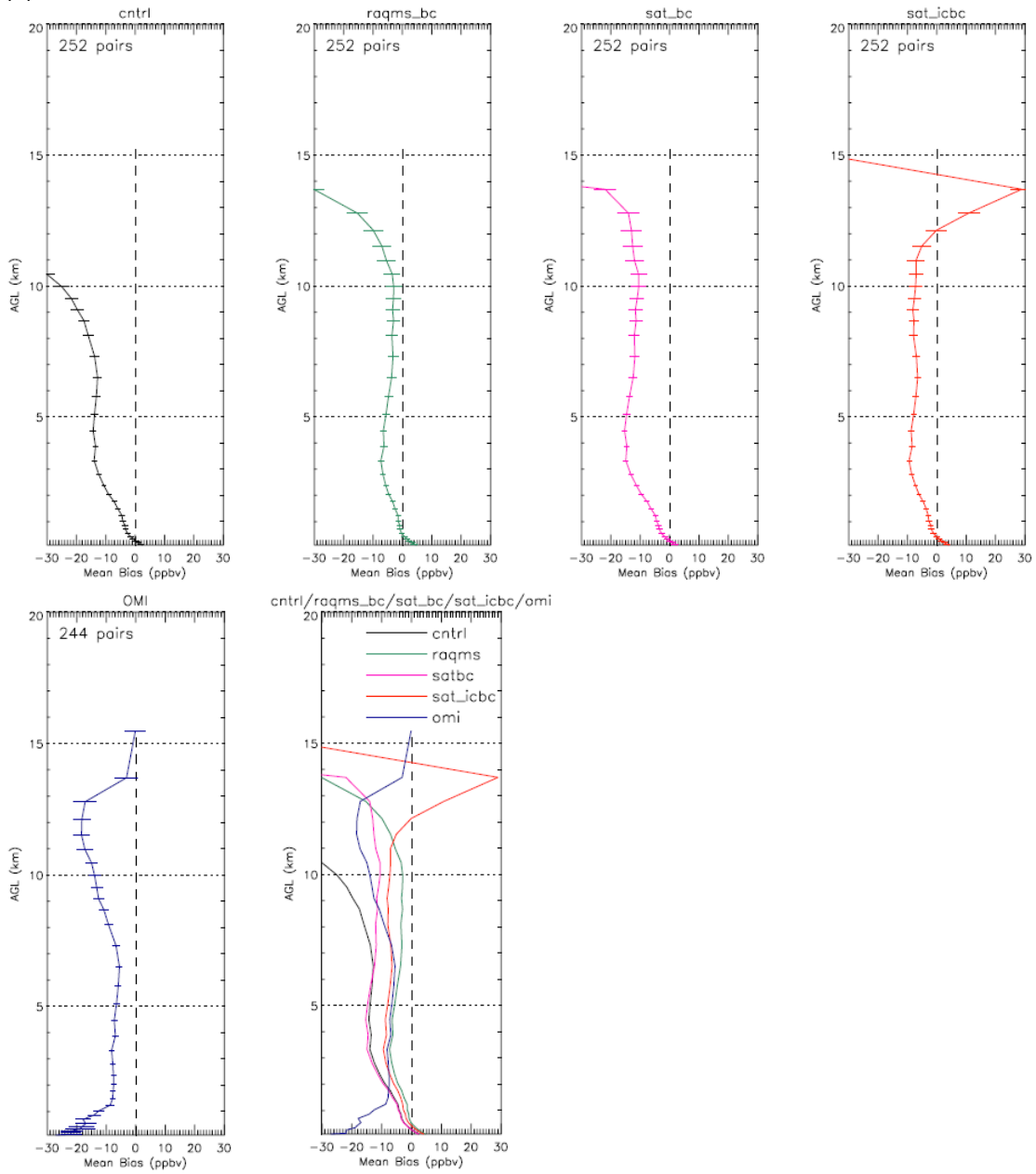


Figure 28- CMAQ-simulated ozone variations at Huntsville, AL, during August 2006. Ozonesonde measurements are re-sampled onto CMAQ vertical resolution and then overplotted onto model simulations.

(a)



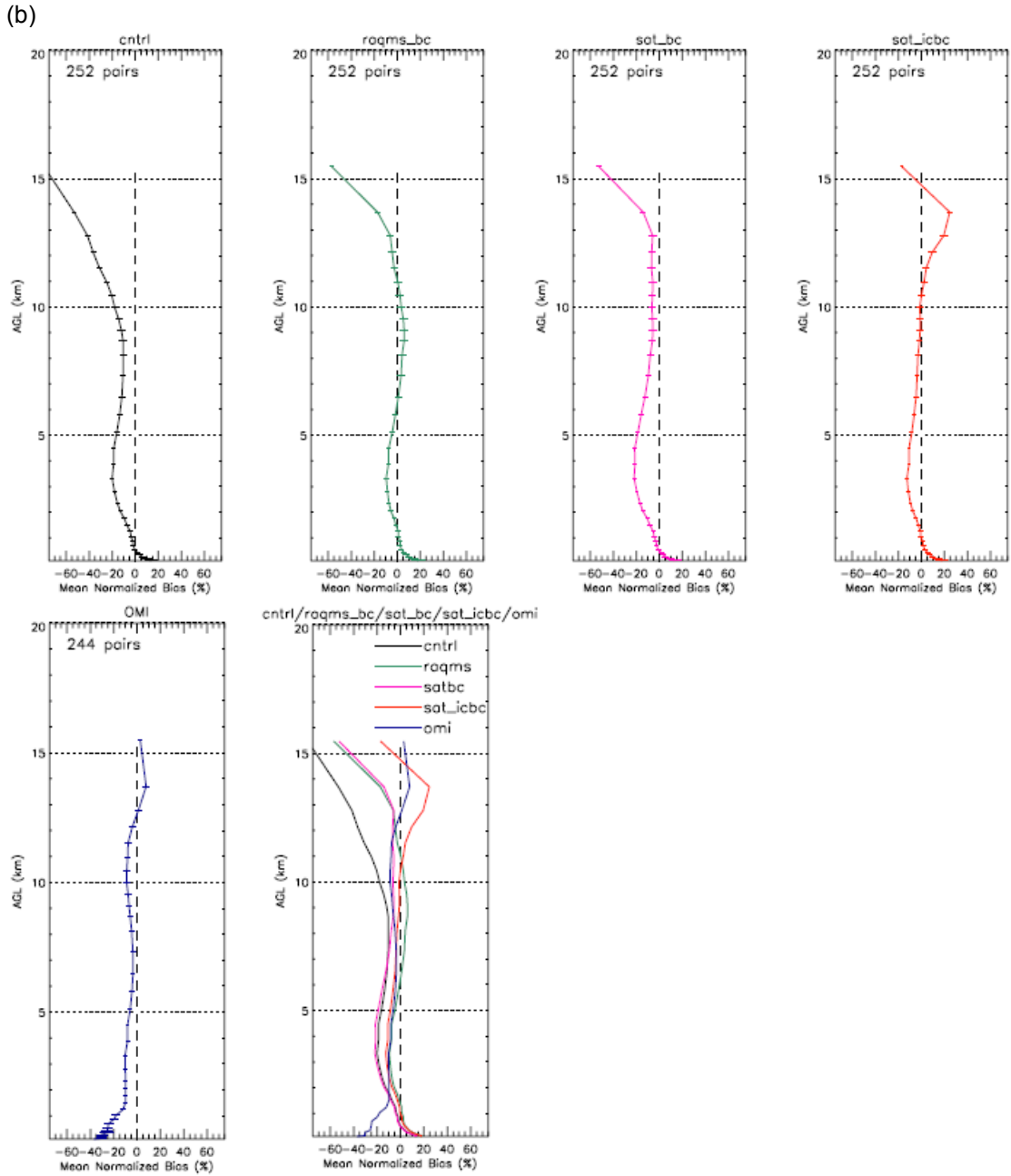


Figure 29- Differences calculated between model simulations (base, RAQMS_bc, sat_bc, sat_icbc) and ozonesondes, as well as between level-2 OMI/O₃ profiles and ozonesondes, during August 2006. (a) Mean bias. (b) Mean normalized bias.

Table 12- sample sizes (number of coincidence pairs between ozonesonde and model simulated ozone profiles/OMI ozone profiles) within each CMAQ layer

Layer #	height (km; AGL)	cntrl	raqms_bc	sat_bc	sat_icbc	OMI
39	15.475	251	251	251	251	243
38	13.698	252	252	252	252	244
37	12.784	252	252	252	252	244
36	12.130	252	252	252	252	244
35	11.530	252	252	252	252	244
34	10.975	252	252	252	252	244
33	10.458	252	252	252	252	244
32	9.974	252	252	252	252	244
31	9.519	252	252	252	252	244
30	9.088	252	252	252	252	244
29	8.679	252	252	252	252	244
28	8.103	252	252	252	252	244
27	7.308	252	252	252	252	244
26	6.506	252	252	252	252	244
25	5.772	252	252	252	252	244
24	5.096	251	251	251	251	243
23	4.469	252	252	252	252	244
22	3.883	252	252	252	252	244
21	3.332	252	252	252	252	244
20	2.813	251	251	251	251	243
19	2.370	250	250	250	250	242
18	2.039	251	251	251	251	243
17	1.765	250	250	250	250	242
16	1.498	249	249	249	249	226
15	1.239	226	226	226	226	87
14	1.028	224	224	224	224	47
13	0.862	226	226	226	226	31
12	0.700	225	225	225	225	22
11	0.540	224	224	224	224	10
10	0.421	226	226	226	226	8
9	0.343	225	225	225	225	7
8	0.266	226	226	226	226	3
7	0.189	224	224	224	224	3
6	0.132	204	204	204	204	3
5	0.094	183	183	183	183	1
4	0.056	176	176	176	176	0
3	0.026	159	159	159	159	0
2	0.011	143	143	143	143	0
1	0.004	127	127	127	127	0

4. Discussion

[*R. B. Pierce, et al., 2007*] examined the effect of such an approach on CMAQ predictions and concluded that while CMAQ predictions in the free troposphere improved, it did not significantly affect surface ozone predictions. More recently, [*Song, et al., 2008*] investigated the impact of boundary conditions developed using global model output such an approach on CMAQ-CTM predictions. Compared to the predefined time-independent boundary condition, the dynamic lateral boundary condition resulted in higher ozone concentrations (up to 200 ppb) in upper levels at high altitudes, and at surface monitors in the Midwest. In the current study, using RAQMS for providing lateral boundary condition served as another reference point in quantifying the impact of using satellite information directly in the regional modeling system versus realizing their impact through their assimilation in a global model.

5. Acknowledgements

We gratefully acknowledge the contributions of Xiong Liu for the AURA/OMI ozone profiles, Daewon Byun and Brad Pierce for the RAQMS CTM boundary conditions, and the IONS06 ozonesonde team for the ozonesounding.

We would also like to thank Crosscutting Solutions Program Manager, Mr. Elbert Lucien Cox, Jr., of the NASA Applied Sciences Program for his guidance throughout this project

G. Conclusions and recommendation for future research and applications

Thus far, we have demonstrated the utility of OMI O₃ profiles and MODIS aerosol products in CMAQ (the Decision Support Tool). OMI O₃ significantly improved model performance in the free troposphere and MODIS aerosol products substantially improved PM_{2.5} predictions.

There are still issues concerning the fact that neither OMI nor TES provide adequate information in the boundary layer with respect to O₃. Our benchmarking efforts have shown marginal improvements in the model performance within the boundary layer. However, with boundary layer O₃ being of particular importance to the air quality community, the future work should devise approaches to better characterize pollution episodes. One approach could include the use of other AURA products such as NO₂, HCHO, and CO. Because the formaldehyde abundance is mainly limited to the boundary layer, column measurements of HCHO can make significant contribution to the better representation of the boundary layer chemical composition.

With respect to the use of aerosol products, while satellite data improved model performance of PM_{2.5} total mass concentration, aerosol speciation remains a challenge. The incorporation of satellite data relied on a key assumption that the aerosol partitioning within the model is reliable. Therefore, revisiting this assumption or improving the aerosol model within the DST takes higher priority.

The current project examined only the impact of the boundary conditions on the air-quality predictions. This limitation implies that the use of the satellite data was helpful in the realization of transboundary transport of pollution and helped in better representation of the free-tropospheric ozone. However, the daily information from the satellite helps improve the initial condition in the model. This effort seems to be the natural extension of the current project and effectively assimilates the satellite data into the model fields. Because the initial conditions greatly affect the short-term predictions, use of satellite data for IC can also potentially improve air-quality forecasts.

Finally, the current project did not examine the role of assimilation in improving the physical atmosphere. A future development of DST should include an improved physical atmosphere in

conjunction with the assimilation of satellite trace gases. Assimilation of satellite-observed clouds greatly improves model predictions of ozone within the boundary layer. It also eliminates one component of inconsistency between the model and the observations.

One of the problems in satellite data assimilation is that the observed physical/chemical world is not always consistent with the model world. Clouds are a major manifestation of this inconsistency. A discrepancy between model clouds (clear sky) and the satellite clouds (clear sky) impacts the radiation fields, vertical transports and local circulations, the chemistry and microphysical properties. This discrepancy implies that when one component of the physical or chemical atmosphere is perturbed (adjusted) by the assimilation of satellite data, the complete environment for supporting and sustaining the adjustment does not exist. Therefore, as we continue to introduce more chemical observations into the modeling framework, it is also essential to model the physical environment more realistically. These improvements include assimilation of satellite observed skin temperature, moisture, albedo, insolation, and clouds in conjunction with the assimilation of trace gases and aerosols.

Another area of interest for DST future development is the inclusion of lightning-generated NO_x (LNO_x) in the emissions inventory. Such an effort can take advantage of AURA's column NO₂ measurements to reduce the uncertainty in LNO_x production rate and the Lightning Imaging Sensor (LIS) observations to complement the National Lightning Detection Network (NLDN) data and better quantify the spatial distribution of LNO_x.

References

- Al-Saadi, J. A., A. Soja, R. B. Pierce, J. Szykman, C. Wiedinmyer, et al. (2008), Intercomparison of near-real-time biomass burning emissions estimates constrained by satellite fire data, *J. Appl. Remote Sens.*, 2, 1-24, DOI: 10.1117/1.2948785.
- Anthes, R. A. and T. T. Warner (1978), Development of hydrodynamic models suitable for air pollution and other mesometeorological studies, *Mon. Wea. Rev.*, 106, 1045-1078.
- Bhave, P. V., S. J. Roselle, F. S. Binkowski, C. G. Nolte, S. Yu, et al. (2004), CMAQ aerosol module development: Recent enhancements and future plans, Proceedings of the 2004 Models-3/CMAQ Conference, Chapel Hill, N.C., 18- 20 October.
- Binkowski, F. S. and S. J. Roselle (2003), Models-3 Community Multiscale Air Quality (CMAQ) model aerosol component: 1. Model description, *J. Geophys. Res.*, 108 (D6), 4183, doi:10.1029/2001JD001409.
- Byun, D. W. and K. L. Schere (2006), Review of governing equations, computational algorithms, and other components of the models-3 Community Multiscale Air Quality (CMAQ) modeling system, *Appl. Mech. Rev.*, 59, 51-77.
- Chang, J. S., P. B. Middleton, W. R. Stockwell, C. J. Walcek, J. E. Pleim, et al. (1990), The regional acid deposition model and engineering model, Acidic Deposition: State of Science and Technology, Report 4, National Acid Precipitation Assessment Program.
- Coats, C. J. Jr. (1996), High-performance algorithms in the Sparse Matrix Operator Kernel Emissions (SMOKE) modeling system.
- DeMore, W. B., S. P. Sander, D.M. Golden, R.F. Hampson, M.J. Kurylo, et al. (1994), Chemical kinetics and photochemical data for use in stratospheric modeling, Evaluation Number 11, 274 pp, JPL, Pasadena, California.
- Dennis, R.L., D.W. Byun, J.H. Novak, K.J. Galluppi, C.J. Coats, et al. (1996), The next generation of integrated air quality modeling: EPA's models-3, *Atmos. Environ.*, 30 (12), 1925-1938.
- Dudhia, J. (1989), Numerical study of convection observed during the winter monsoon experiment using a mesoscale two-dimensional model., *J. Atmos. Sci.*, 46, 3077-3107.
- Emery, C. A.E. Tai and G. Yarwood (2001), Enhanced Meteorological Modeling and Performance Evaluation for Two Texas Ozone Episodes, Texas Natural Resource Conservation Commission, ENVIRON International Corp, Novato, CA.

- Grell, G. A. J. Dudhia and D. R. Stauffer (1995), A Description of the Fifth-Generation Penn State/NCAR Mesoscale Model (MM5). NCAR Technical Note NCAR/TN-398+STR, National Center for Atmospheric Research, Boulder, CO.
- Guenther, A. , C. Geron, T. Pierce, B. Lamb, P. Harley, et al. (2000), Natural emissions of non-methane volatile organic compounds, carbon monoxide, and oxides of nitrogen from North America, *Atmos. Environ.*, *34*, 2205-2230.
- Hand, J. L. and W. C. Malm (2005), Review of the IMPROVE equation for estimating ambient light extinction coefficients, National Park Service and Colorado State University.
- Houyoux, M., J. Vukovich, C. Coats Jr., N. Wheeler, and P. Kasibhatla (2000), Emission inventory development and processing for the Seasonal Model for Regional Air Quality (SMRAQ) project, *J. Geophys. Res.*, *105 (D7)*, 9079-9090.
- Otte, T. L., A. Lacser, S. Dupont, and J. K. S. Ching (2004), Implementation of an urban canopy parameterization in a mesoscale meteorological model, *J. Appl. Meteor.*, *43*, 1648-1665.
- Pierce, R. B., J. A. Al-Saadi, T. Schaack, A. Lenzen, T. Zapotocny, et al. (2003), Regional Air Quality Modeling System (RAQMS) predictions of the tropospheric ozone budget over east Asia, *J. Geophys. Res.*, *108 (D21)*.
- Pierce, R. B., T. Schaack, J. A. Al-Saadi, T. D. Fairlie, C. Kittaka, et al. (2007), Chemical data assimilation estimates of continental U.S. ozone and nitrogen budgets during the Intercontinental Chemical Transport Experiment–North America, *J. Geophys. Res.*, *112 (D12S21)*, doi:10.1029/2006JD007722.
- Pierce, T., C. Geron, L. Bender, R. Dennis, G. Tonnesen, et al. (1998), Influence of increased isoprene emissions on regional ozone modeling, *J. Geophys. Res.*, *103 (D19)*, 25,611-25,629.
- Song, C.-K., D. W. Byun, R. B. Pierce, J. A. Al-Saadi, T. K. Schaack, et al. (2008), Downscale linkage of global model output for regional chemical transport modeling: Method and general performance, *J. Geophys. Res.*, *113 (D08308)*, doi:10.1029/2007JD008951.